Division of Solid Mechanics

ISRN LUTFD2/TFHF--06/5117--SE (1-85)

TOPOLOGY OPTIMIZATION OF A STAMPING DIE

Master's Dissertation by

Frida Birath and Anna Nilsson

Supervisors
Håkan Carlsson, Altair Engineering
Mats Sigvant, Volvo Cars Body Components
Mathias Wallin, Div. of Solid Mechanics
Magnus Fredriksson, Div. of Solid Mechanics

For information, address:
Division of Solid Mechanics, Lund University, Box 118, SE-221 00 Lund, Sweden.
Homepage: http://www.solid.lth.se

Acknowledgment

This Master's thesis was carried out at Altair Engineering AB and at the Division of Solid Mechanics at Lund Institute of Technology from September 2005 to January 2006.

We would like to express our appreciation to supervisor Ph.D. Håkan Carlsson at Altair for inspiration and guidance throughout the project. We would also like to thank Ph.D. Mats Sigvant at Volvo Cars Body Component for valuable information and insightful remarks.

Our supervisors at the Division of Solid Mechanics, Ph.D. Mathias Wallin and Doctoral candidate Magnus Fredriksson, have provided us with helpful discussions and feedback throughout the project, thank you! Doctoral candidate Linus Larsson has also been helpful and provided essential information on sheet metal forming.

We would also like to express our deepest gratitude to the staff at Altair for their help, support and everlasting patience. Without your assistance, this work would have been difficult to achieve.

Lund, May 2006
Frida Birath and Anna Nilsson

Abstract

Today the casting structure of stamping tools is dimensioned according to standard guidelines. The main task of this thesis is to develop an alternative method of manufacturing stamping tools, which takes the structural response of the tool into account to produce a lightweight design. This is done by performing a topology optimization with the objective to improve the structural stiffness and to reduce the weight of the tool.

The die is the only part of the stamping tool considered in the methodology generation. The method established can be applied to any other part of the stamping tool analogously, after the load cases of the part are determined. Two different load cases are applied to the die tool, one operation case and one transportation case, which are weighted equally when optimizing. A forming simulation is made using LS Dyna to obtain the load on the die during operation. The attained loads are, together with the loads affecting the die during transportation, applied to the die and a topology optimization is performed, using the software OptiStruct.

A CAD model is set up from the result of the topology optimization. This CAD model is analysed and compared to the original die, i.e. the die that is in use today. When comparing the result of the analyses, the maximal displacement, the von Mises stresses and the weight of the die is considered. The final results show an overall more homogenous distribution of displacement, a reduction of the maximal displacement with around 30 % and a weight reduction of about 20 %.

Table of Contents

Chapter 1

Introduction

Volvo Cars Body Components (from now on *VCBC*), has great experience in tool design and sheet metal forming. They are situated in Olofström, Sweden, where there has been sheet stamping industry since 1735. Body components for the first Volvo car where produced in Olofström in 1927. In 1969 Volvo Car Corporation purchased the plant in Olofström and today VCBC is *Volvo Cars Centre of Excellence for Forming of Metallic Materials*.

1.1 Background

The lead time for development of new car models has been considerably reduced over the years, thanks to outstanding practical experience, combined with focus on experimental research and finite element sheet forming simulations. The development has also lead to use of body component materials of greater and higher strength, which calls for a greater force to be used in the forming process. More material has traditionally been applied to the stamping tool for it to sustain this increased load, and in order to reduce the risk of a large structural response. However, this course of action cannot carry on indefinitely, since the lifting capacity of traverse cranes, needed for transporting the tools in the plant, is limited and soon reached. Therefore an alternative method of manufacturing tools, which takes the structural response of the tool into account to produce a lightweight design, is called for.

1.2 Problem Description

For hundreds of years sheet metal forming has been done using stamping (for more details, see section 2.1). The experience gained has helped to improve the design of the tool over the years. Today, the casting structure of the tool is dimensioned according to standard guidelines. These guidelines are based on trial-and-error and not

on a structural optimization, i.e. further improvements with respect to structural stiffness and reduction of weight of the tool should be attainable.

1.3 Objective

The aim of this project is to generate a method for a manufacturing process of stamping tools, which takes the structural response of the tool into account, while reducing its weight. The purpose is to carefully investigate the different steps of the method which are

1. Generate a mesh on the structure
2. Define the loads and constraints on the tool
3. Set up and perform a topology optimization
4. Re-design the tool according to the result of the topology optimization

1.4 Delimitations

The method is applied to the tool forming of the Volvo S80 truck lid. Only one tool part, the die, is being optimized in this project. The optimized form of the other tool parts may be derived analogously.

Only the first press in the press line, where the sheet metal forming takes place, is considered. The method of this thesis can be applied to other kinds of presses (see section 2.3), but only after the unique load cases of this particular press has been established.

The loads established from the last time step of the sheet metal forming simulations are applied on the die for topology optimization. One may consider using more than one time step to illustrate the actual dynamic load, however, this will not be done.

The loads applied on the die can be considered as perfect since the moving part of the tool follows the z-axis. In reality there is no such thing as a perfect load and one may consider taken this into account.

Only one kind of topology optimization problem is set up, with the objective to give the structure a maximum stiffness given a certain available amount of material volume, i.e. the weight is constrained. There are numerous other possibilities, for example to minimize the weight of the structure for a given structural response. However, this kind of topology optimization is not carried out.

Since the aim of this project is to reduce weight and increase the stiffness of the die, a cost reduction can be achieved, which ultimately may lead to increasing profits. However, this kind of economical study will not be performed.

1.5 Disposition

This report starts with a theoretical review of sheet metal forming, continuum mechanics, topology optimization and time integration methods in chapter 2 till 5. Continuing, the methodology of the project is presented in chapter 6 till 9. And finally, the results are presented and analysed in the final chapters, chapter 10 till 12.

Chapter 2

Sheet Metal Forming

The truck lid considered is manufactured in a forming process. The contact pressure resulting from this stamping process is calculated to get the load on the die, necessary for the topology optimisation. To get a better understanding of this manufacturing process, a brief introduction to sheet metal forming will be given. For more information, the reader may consult Schuler Metal Forming Handbook [2].

2.1 Tool Set up

Sheet metal forming is a manufacturing process with the purpose of forming a sheet blank through plastic deformation. The tools may vary slightly in their assembly but normally they consist of a die, a punch and a blankholder. The die and the punch can also be referred to as lower and upper die, respectively. In the tool, a drawbead might be present with the objective of restraining the blank and thereby reducing the required blankholder force, see fig 2.1 below.

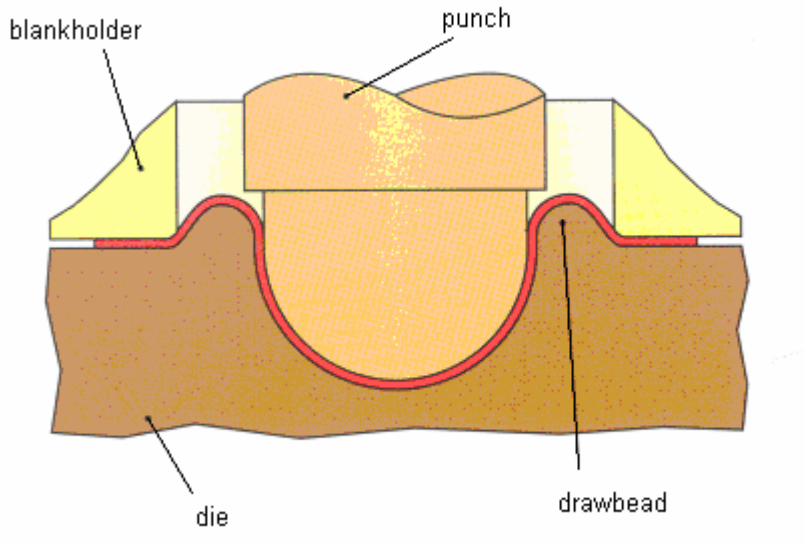

Fig 2.1 Tool set up in sheet metal forming

A complete tool consists of a pair of mating members, the die and the punch, including all supporting and actuating parts of the tool. The upper members are attached to the slide of the press, while the lower member is clamped or bolted to the bolster of the press.

The blankholder controls the metal flow around the shape to be formed in the draw operation. The undeformed blank is designed to facilitate forming and to eliminate a trimming operation subsequent to forming.

A drawbead is a ridge placed around a portion of the die cavity, or all around it, to control blank forming. A groove in the mating blankholder allows the two mating parts to close. The drawbead forces the blank to bend and unbend several times while it is pulled through the bead, which restrains the blank and increase the plastic deformation of the part.

2.2 Stretch Forming vs. Deep Drawing

In stretch forming the blank is prevented from sliding into the die, either by a drawbead or by applying a sufficiently high blankholder force, which makes the blankholder work as a break. As a result, the blank is subjected to tensile stress when interacting with the punch, which will reduce the sheet metal thickness. The localized thinning that occurs prior to fracture is called necking, see fig 2.2a.

In contrast, deep drawing is a forming process under combined tensile and compressing conditions without altering the thickness of the blank. The main purpose of the blankholder is to prevent wrinkles to form, by applying a force that makes the blank glide in an appropriate manner, see fig 2.2b.

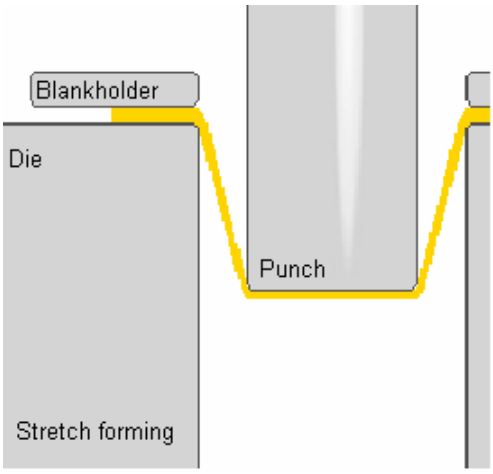

Fig 2.2a Stretch forming

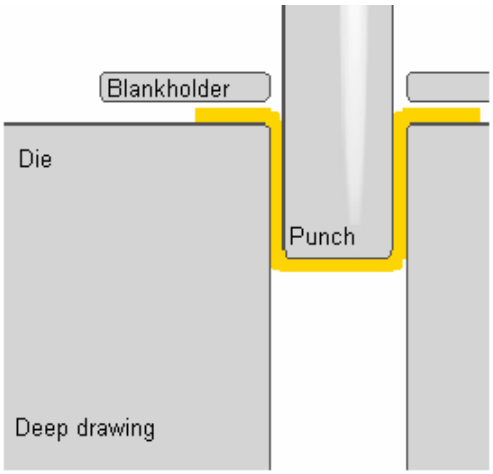

Fig 2.2b Deep drawing

In practice, a combination of stretch forming and deep drawing is conducted simultaneously. The blank thickness can remain unchanged, or can be reduced in some specified parts. The main difficulty in this combined forming process is to establish an acceptable compromise between wrinkling, caused by a low blankholder force, and rupture, caused by a large blankholder force.

2.3 The Press Line

The manufacturing process can be seen as a series of operations such as forming, flanging, piercing and cutting. These operations are assembled together in a press line. The VCBC plant consists of twenty press lines that all contains coilfeeder, straightener, shear, robots and usually five presses. The coilfeeder feeds the metal coil into the straightener, which keeps the coil straight. The shear cuts the coil into sheets, which the robot puts in, and takes out of the press. See fig 2.3 for more details.

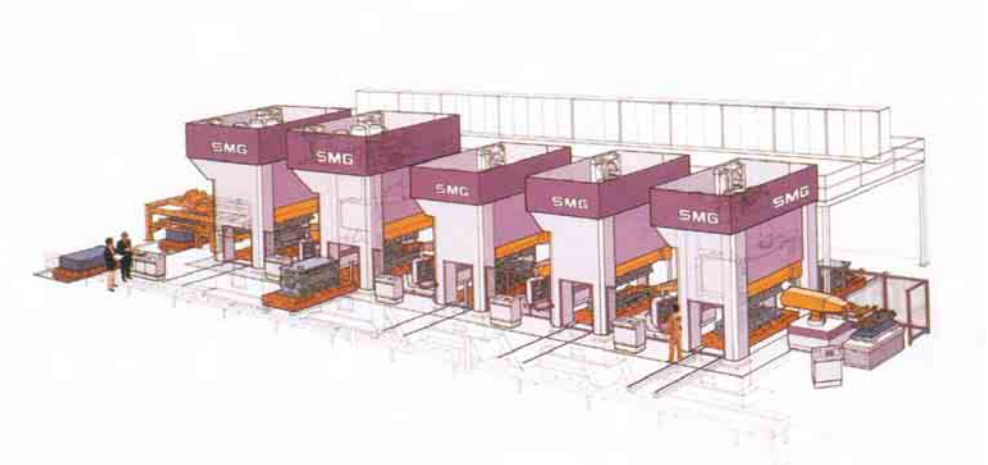

Fig 2.3 The press line

2.4 Standard Manufacturing Guidelines

The tool is manufactured by casting in a disposable mould. The draw direction still needs to be considered, in order to ensure that all mould parts are removable. Nevertheless, there are yet some technical aspects of casting to be taken into account. The VCBC standard guidelines [1] state that ribs and other reinforcements should not meet at sharp angles. This is to avoid material concentration, which results in an inhomogeneous structure and lower strength. Also, the ribs should be designed in a staggered way to reduce the risk of distortion and cracking during the casting process, see the fig below.

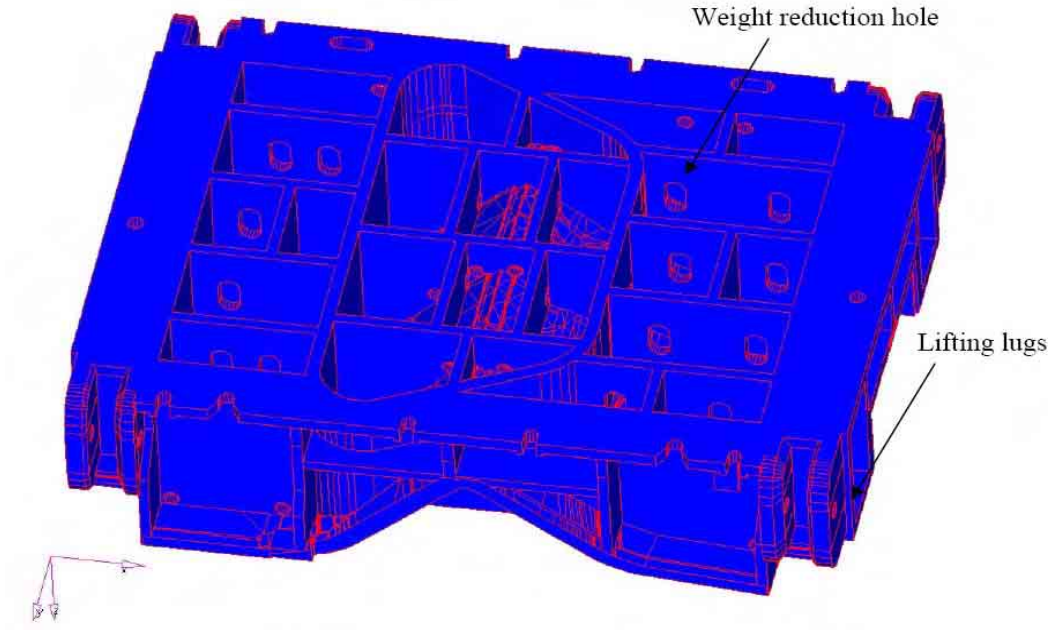

Fig. 2.4 The rib framework of the original die

Fig 2.4 shows the bed-side of the die considered in this project. It also sets an example of a standard framework of walls and compartments in a press die. To achieve sufficient strength, the distance between the compartment walls must be adapted to the depth of the compartment, i.e. the shallower the compartment, the shorter the distance should be between the walls of the compartment. This is because narrow and deep compartments cannot be casted in a satisfactory manner. The thickness of the walls is also of importance, since too thin sections will lead to stress concentration and risk of cracking, whereas a too thick section will have an incorrect solidification sequence.

Lifting lugs are attached to all parts of the stamping tool to facilitate transport. They can be designed either integrated with the die or on the outside of the die. When possible, the lifting equipment should be placed at half the height of the die section, i.e. near its centre of gravity, to make sure that the tool is balanced in a vertical position. The lifting lugs should be located above each other in direct alignment in the upper and lower die.

2.5 Forming Limit Diagram

A Forming Limit Diagram (FLD) is a graphical representation of the in-plane principal strains in a part. It is used to detect forming defects, such as failure by tearing or wrinkling. The empirically or theoretically established Forming Limit Curves (FLC) shows the biaxial strain levels beyond which failure may occur in sheet metal forming, i.e. the FLC is describing the formability if the blank material. The strains are given in terms of major and minor strains that are measured from deformation of circles, which previously have been printed onto the undeformed sheet. The comparison of measured deformations with the FLD gives an estimation of the risk of failure during the stamping process.

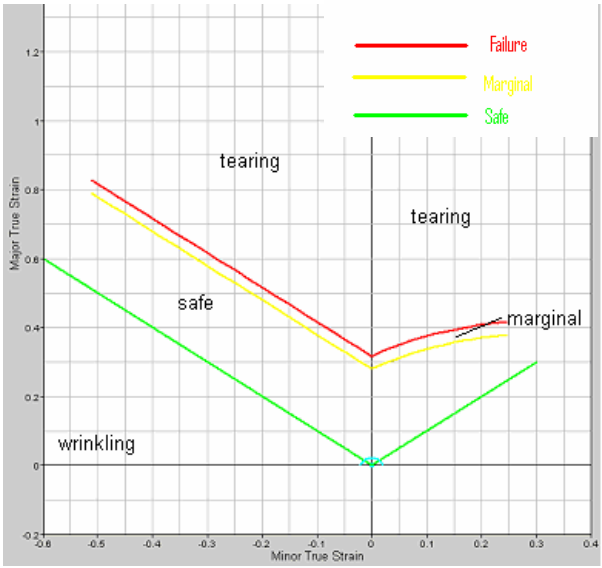

Fig 2.5 Forming limit diagram

A combination of major and minor strains will fall in one of three zones, safe, marginal, or failure. If a measured deformation gives a point representing a major and minor strain combination that lies below the marginal curve, it is in the safe zone and breakage during stamping should not be expected. However, if the absolute value of the minor principal strain is larger then the major principal strain, there will be wrinkles in the panel, which is sometimes unacceptable due to part quality demands or risk of extreme die wear. If a point lies within the area between the marginal and failure curve, it is in the marginal zone; and periodic breakage may occur if the variation in process parameters is sufficient to create strains high enough to move the location into the failure zone. Points lying above the band are in the failure zone, and breakage will be a frequent problem. A die or lubrication change is generally required to remedy such a problem. The shape of the FLD is quantitatively the same for all steels. The curve moves up and down the major strain axis as a function of steel sheet characteristics. The location of the curve is dependent on the thickness, strain-hardening exponent (n-value) and the ductility of the material. The strain hardening exponent is derived from the relationship between true stress, σ, and true strain, ε

$$\frac{\sigma}{\sigma_0} = K\left(\frac{\varepsilon}{\varepsilon_0}\right)^n \tag{2.1}$$

giving a measure of the stretchability of the steel. The strain-hardening exponent may have values from n = 0, giving an ideal plastic solid, to n = 1, representing an elastic solid.

Chapter 3

Continuum Mechanics

The forming process described in the previous chapter will later be simulated through finite element analysis. The deformable sheet has been given anisotropic material properties when being manufactured through rolling. In the FE-model of the forming process the Hill plasticity material model will be used to simulate the anisotropic behaviour of the sheet and will therefore be presented in this chapter. The interested reader may consult Ottosen and Ristinmaa [3] - [4] for more details.

3.1 Kinematics

When dealing with large deformations it is useful to relate the displacements to a reference configuration [4]. The reference configuration is the condition of the body before load has been applied to it. At time $t = 0$, the position vector of a particle is described by the coordinates **X**=(X,Y,Z) in a fixed coordinate system. The position of the same particle at time t is described by the position vector **x** =(x,y,z) in the same coordinate system. See figure 3.1. We note that the relationship between the two position vectors in space is the displacement vector **c**.

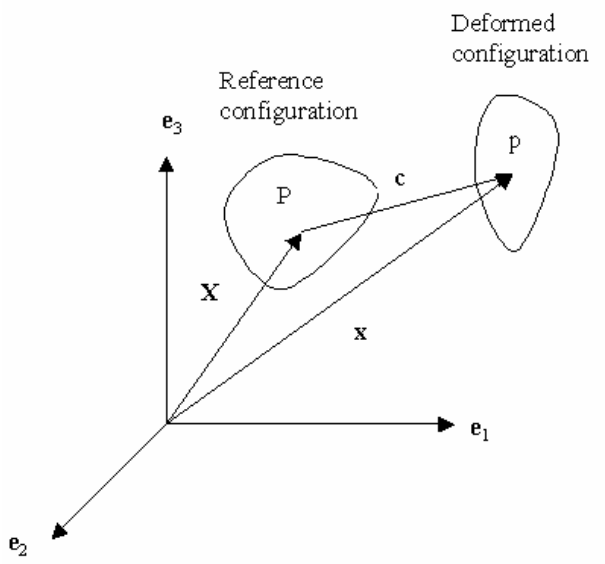

Fig. 3.1 Reference and deformed configuration

At a fixed time, we can directly write the relationship between the spatial coordinates **x** and the material coordinates **X** through vector addition:

$$\mathbf{x} = \mathbf{x}(\mathbf{X}, t) = \mathbf{X} + \mathbf{c}(\mathbf{X}, t) \tag{3.1}$$

This description of the motion is termed a Lagrangian description, where $\mathbf{c}(\mathbf{X}, t)$ is the displacement vector denoted as $\mathbf{c} = (c_x, c_y, c_z)$. The distance between two neighbouring particles in the reference configuration is defined as $d\mathbf{X}$, and the distance between two neighbouring particles in the deformed configuration is defined as $d\mathbf{x}$. The relation between $d\mathbf{X}$ and $d\mathbf{x}$ can be written as

$$d\mathbf{x} = \mathbf{F} d\mathbf{X} \tag{3.2}$$

where **F** is the deformation gradient tensor defined as

$$F_{ij} = \frac{\partial x_i}{\partial X_j} \tag{3.3}$$

The velocity of a material particle can be expressed as

$$\mathbf{v} = \frac{\partial \mathbf{x}}{\partial t} \tag{3.4}$$

The velocity difference between two neighbouring particles in the deformed configuration is described as

$$d\mathbf{v} = \frac{\partial \mathbf{v}}{\partial \mathbf{x}} d\mathbf{x} = \mathbf{L} d\mathbf{x} \tag{3.5}$$

where **L** is the spatial velocity gradient in the deformed configuration. Equation 3.5 can, using equation 3.2, be expressed as

$$d\mathbf{v} = \mathbf{L} d\mathbf{x} = \mathbf{L}\mathbf{F} d\mathbf{X} \tag{3.6}$$

The velocity difference can also be obtained from equation 3.4 and 3.2 by

$$d\mathbf{v} = \frac{\partial}{\partial t}\left(\mathbf{F} d\mathbf{X}\right) = \dot{\mathbf{F}} d\mathbf{X} \tag{3.7}$$

where

$$\dot{\mathbf{F}} = \frac{\partial \mathbf{F}}{\partial t} \tag{3.8}$$

Equation 3.6 and 3.7 is compared and it is seen that

$$\dot{\mathbf{F}} = \mathbf{L}\mathbf{F} \tag{3.9}$$

L can be split into one symmetric part **D** and one antisymmetric part **W** according to

$$\mathbf{L} = \mathbf{D} + \mathbf{W} \tag{3.10}$$

where **D** is the rate of deformation tensor defined as

$$\mathbf{D} = \frac{1}{2}\left(\mathbf{L} + \mathbf{L}^T\right) \tag{3.11}$$

and **W** is the spin tensor defined as

$$\mathbf{W} = \frac{1}{2}\left(\mathbf{L} - \mathbf{L}^T\right) \tag{3.12}$$

To define a strain measure, the change of length in a material vector is going from the reference configuration to the deformed configuration. The length of vector $d\boldsymbol{x}$ is denoted as ds and the length of vector $d\boldsymbol{X}$ is denoted dS. The lengths can be measured as

$$dS^2 = d\mathbf{X}^T d\mathbf{X} \tag{3.13}$$

$$ds^2 = d\mathbf{x}^T d\mathbf{x} \tag{3.14}$$

Using equation 3.2, 3.14 can be written as

$$ds^2 = d\mathbf{X}^T \mathbf{F}^T \mathbf{F} d\mathbf{X} \tag{3.15}$$

and it follows that

$$ds^2 - dS^2 = d\mathbf{X}^T \left(\mathbf{F}^T \mathbf{F} - \mathbf{I}\right) d\mathbf{X} \tag{3.16}$$

which can be written as

$$ds^2 - dS^2 = 2d\mathbf{X}^T \mathbf{E} d\mathbf{X} \tag{3.17}$$

where the strain tensor **E** is expressed in terms of the deformation gradient tensor **F** as

$$\mathbf{E} = \frac{1}{2}\left(\mathbf{F}^T \mathbf{F} - \mathbf{I}\right) \tag{3.18}$$

The above strain tensor is known as the Green-Lagrange's strain tensor and gives information about the deformations in a body.

3.2 Rate of Deformation Tensor

The Green-Lagrange's strain tensor provides a complete description of the deformation of a body given the material used, independently of rigid body motions. For more details, see Ottosen and Ristinmaa [4]. In some applications it is not the total change of deformation that is of importance, but rather the time rate at which these changes occur. This is the case of plasticity models. In elasto-plasticity the constitutive equations are formulated in rate form. A tensor which describes the rate at which the deformation occurs is the rate of deformation tensor $\mathbf{D}$.

3.3 Plasticity

Plasticity has a time independent behaviour, which is non-linear and were the strains are partly preserved when the material is unloaded. These remaining strains are the plastic strains. Plasticity occurs when the material is exposed to loads that develop stresses higher than the yield stress of the material, which means that the yield stress is the minimum stress required to permanently deform a material. No unique relation exists between the stress state and the strain state in plasticity. For a given strain state, the corresponding stress state is obtained by an integration of the incremental constitutive relations and the result of this integration will depend on the load history. For more details on continuum mechanics, see Ottosen and Ristinmaa [3]

3.4 Small Strain Plasticity

In general, the yield stress varies with the plastic deformation. Since the yield surface is a generalization of the yield stress, for a general stress state it is evident that the yield surface will change with the plastic loading. This change of yield surface is called the hardening rule.

The yield surface is described by

$$f\left(\boldsymbol{\sigma}, K^{\alpha}\right) = 0 \quad \alpha = 1,...,n \tag{3.19}$$

where $K^1, K^2, ...K^\alpha$ are hardening parameters, which characterize the manner in which the current yield surface changes in size, shape and position with plastic loading. For $f < 0$ the response is elastic and for $f = 0$ plastic deformation may occur.

Before any plasticity is initiated, we have per definition that $K^\alpha = 0$. When the hardening parameters are zero, the current yield surface coincides with the initial yield surface. The hardening parameters K^α vary with the plastic load, and to model this, we assume that there exist some internal variables that characterize the state of elastic-plastic material. This means that we can assume that

$$K^\alpha = K^\alpha\left(\kappa^\beta\right) \tag{3.20}$$

where $\kappa^\beta = \text{internal variables}, \left(\beta = 1,2,...\right)$. The number of hardening parameters equals the number of internal variables since the relation between K^α and κ^β is unique. The important point is that the internal variables are used to memorize the plastic loading history, and because of this, they are zero before any plasticity is initiated.

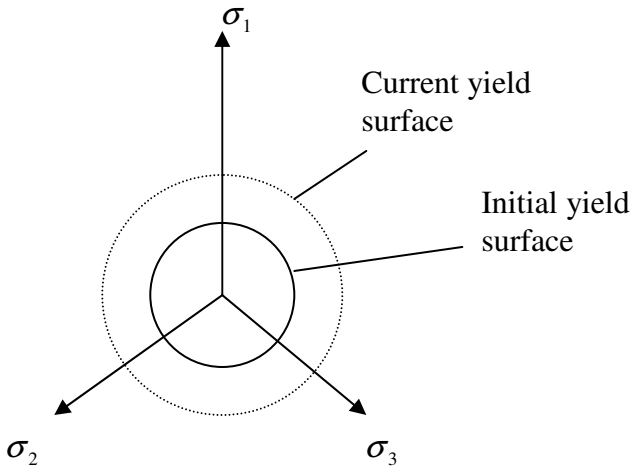

Fig. 3.2 Isotropic hardening of the von Mises criterion in deviatoric plane

In the case where the small assumption applies one can decompose the total strain tensor into one elastic part and one plastic part given by

$$\boldsymbol{\varepsilon} = \boldsymbol{\varepsilon}^e + \boldsymbol{\varepsilon}^p \tag{3.21}$$

The strain variation over time can be expressed as the strain rate

$$\dot{\boldsymbol{\varepsilon}} = \dot{\boldsymbol{\varepsilon}}^e + \dot{\boldsymbol{\varepsilon}}^p \tag{3.22}$$

where $\dot{\boldsymbol{\varepsilon}}^e$ is the elastic strain rate and $\dot{\boldsymbol{\varepsilon}}^p$ is the plastic strain rate.

The elastic strains are determined from Hook's law, i.e.

$$\boldsymbol{\sigma} = \tilde{\mathbf{D}}\left(\boldsymbol{\varepsilon} - \boldsymbol{\varepsilon}^p\right) \tag{3.23}$$

where $\tilde{\mathbf{D}}$ is the elastic stiffness tensor.

The associated flow rule for the plastic strain is obtained

$$\dot{\boldsymbol{\varepsilon}}^p = \dot{\lambda}\frac{\partial f}{\partial \boldsymbol{\sigma}} \tag{3.24}$$

and the yield surface serves as a potential function for the determination of the incremental plastic strains. This means that the inelastic part of the deformation is defined by the flow rule. The direction of $\dot{\boldsymbol{\varepsilon}}^p$ is given by the gradient $\frac{\partial f}{\partial \boldsymbol{\sigma}}$. $\dot{\lambda}$ is called the plastic multiplier and determined from the consistency condition $\dot{f} = 0$. If $\dot{\lambda} = 0$ no plastic strains will develop in the material. A more general format of law 3.24 is obtained if *f* is changed into a general potential function *g*. This format is referred to as the non-associated format.

3.5 Simple Plasticity Model for Large Deformations

The problem with the plasticity models for large deformations is that it is not possible to make a decomposition of the strain as done in equation 3.21. Because of this, the rate of deformation, described in section 3.2, is used instead and can be written as

$$D = D^e + D^p \tag{3.25}$$

For an isotropic material the shape and position of the yield surface remain fixed, whereas the size of the yield surface changes. This situation is called isotropic hardening. Here, the isotropic hardening criterion by von Mises will be considered. Hill plasticity, which will be used in this project, is a generalization of the von Mises criterion to anisotropic materials.

The yield surface is given by

$$f\left(\boldsymbol{\sigma}, K^{\alpha}\right) = \left(3J_2\right)^{1/2} - \sigma_y\left(\kappa\right) = 0 \tag{3.26}$$

J_2 is a generic invariant of the stress deviator tensor $\mathbf{s}$,

$$J_2 = \frac{1}{2}\mathbf{s}^T\mathbf{s} \tag{3.27}$$

$$\mathbf{s} = \boldsymbol{\sigma} - \frac{1}{3}trace\left(\boldsymbol{\sigma}\right)\mathbf{I} \tag{3.28}$$

where $\mathbf{I}$ is the unit matrix. For more information in this area see [3].

A generalization of (3.24) results in

$$\mathbf{D}^p = \dot{\lambda}\frac{\partial f}{\partial \boldsymbol{\sigma}} \tag{3.29}$$

The effective plastic strain rate, D^p_{eff} is introduced as

$$D_{eff}^{p} = \left(\frac{2}{3} \left(\mathbf{D}^{p} \right)^{T} \mathbf{D}^{p} \right)^{1/2} \tag{3.30}$$

Using (3.26) and (3.29) along with (3.30) results in

$$D_{eff}^{p} = \dot{\lambda} \tag{3.31}$$

Strain hardening is assumed, which means that the hardening parameter κ is given by

$$\kappa = \int D_{eff}^{p} \, dt \tag{3.32}$$

Von Mises criterion of isotropic hardening described above, has been generalized by Hill and this generalization will be presented below.

3.6 Elasticity

In the present work an isotropic hyper elastic model is used to describe the recoverable deformation. The model is based on a Jaumann-rate formulation $\hat{\sigma} = 2 : D^{e}$. For a complete description we refer to LS Dyna User's Manual [6].

3.7 Model for Hill Plasticity

As mentioned earlier, the model for Hill plasticity will be used in this project. It is a generalization of the von Mises criterion to anisotropic materials, which is described above.

The yield surface for Hill plasticity is given by

$$f(\boldsymbol{\sigma}, K) = \left(\sigma_{y0}^{2} \mathbf{s}^{T} \mathbf{P} \mathbf{s} \right)^{1/2} - \sigma_{y0} - K(\kappa) \tag{3.33}$$

The constant material parameter is defined by

$$\sigma_{y0} = \left[\frac{3}{2(F+G+H)} \right]^{1/2} \tag{3.34}$$

$\mathbf{s}$ represents the deviatoric stress and the symmetric matrix $\mathbf{P}$ is defined as

$$\mathbf{P} = \begin{bmatrix} \tilde{\mathbf{P}} & \mathbf{0} \\ \mathbf{0} & \tilde{\mathbf{Q}} \end{bmatrix} \tag{3.35}$$

where

$$\tilde{\mathbf{P}} = \begin{bmatrix} F+G & -F & -G \\ -F & F+H & -H \\ -G & -H & G+H \end{bmatrix} \quad ; \quad \tilde{\mathbf{Q}} = \begin{bmatrix} 2L & 0 & 0 \\ 0 & 2M & 0 \\ 0 & 0 & 2N \end{bmatrix} \tag{3.36}$$

F,G,H,L,M and N are material constants found by empirical testing.

Chapter 4

Structural Optimization

A structure is an assemblage of materials with the purpose to sustain loads. Designing a structure is an iterative process where the design is modified until it complies with the requirements set upon it. This iteration process can be formulated as an optimization problem where the optimal solution is the best of all the designs that fulfils the requirements.

4.1 General Structural Optimization Problem

A general structural optimization problem aims to determin the optimal value of the design variables, $\mathbf{x}$, such that they maximize or minimize the objective function, f, while satisfying the constraints. There are three kinds of constraints; *state constraints*, which are given by an equilibrium, *behavioral constraints* that are upper and/or lower bounds on the displacements or stresses and, finally, there are *geometrical constraints*, specifying bounds on the design variables such as cross-sectional areas. In a continuous optimization problem the design variables may take any value $\mathbf{x} \in \mathbf{R}^n$. To conclude, the optimization problem can be formulated as

$$\begin{aligned} &\text{objective function} && \min_{\mathbf{x}} f(\mathbf{x}) \\ &\text{constraints} && \begin{cases} g_i(\mathbf{x}) \le 0 & \text{for } i = 1,\ldots,m \\ h_j(\mathbf{x}) = 0 & \text{for } \mathrm{j} = 1,\ldots,n \\ \mathbf{x} \in \mathrm{R}^n \end{cases} \end{aligned} \tag{4.1}$$

The solution of the problem is given by a so-called feasible point $\mathbf{x}^*$ such that $f(\mathbf{x}) \ge f(\mathbf{x}^*)$ for all other $\mathbf{x}$.

Structural optimization can be divided into three categories; size optimization, shape optimization and topology optimization. What kind of optimization that is being

conducted depends on the properties of the design variables. In *size optimization* the design variables are some sizing parameters, for example the cross-section area of a beam. The design variables of *shape optimization* are parameters that control the shape of (a part of) the boundary of the design domain. In order to perform a shape optimization a parameterization of the design domain is needed. In *topology optimization* the optimal distribution of material in the design domain is determined. The structure is free to take any shape within a given design domain, finding the optimal shape of external and internal boundaries of the structure and the number of holes in it.

4.2 Topology Optimization

In this project, the stiffness of a stamping die will be optimized by topology optimization, which therefore will be covered in greater detail. The methodology of topology optimization is illustrated by solving a problem of maximization of the stiffness of a linear elastic structure. For more details on topology optimization, and their application, see Bendsøe and Sigmund [5].

4.2.1 State Problem

We consider an open, bounded and connected domain Ω with a smooth boundary Γ, divided into two parts; Γ_u, where the displacement is prescribed and Γ_t , where the traction vector $\mathbf{t}$ is prescribed. The small strain tensor is given by

$$\boldsymbol{\varepsilon}(\mathbf{u}) = \frac{1}{2}(\nabla \mathbf{u} + \nabla \mathbf{u}^T) \tag{4.2}$$

in which $\mathbf{u}$ is the displacement field on Ω. In linear elasticity Hooke's law gives the stresses

$$\begin{aligned} \boldsymbol{\sigma} &= \mathbf{E}\boldsymbol{\varepsilon}(\mathbf{u}) \\ \mathbf{E} &= \mathbf{E}(\mathbf{x}) \end{aligned} \tag{4.3}$$

where **σ** is the stress tensor and **E** is the constant stiffness tensor. The stiffness is allowed to vary within the domain. The state problem is now set as an elliptic boundary value problem, which implies that for given body forces **b** and given traction vector **t** on the boundary part Γ_t, the problem is solved for the displacement field **u**

$$\begin{aligned} \nabla\boldsymbol{\sigma} - \mathbf{b} &= \mathbf{0}, \quad \text{in } \Omega \\ \mathbf{u}_i - \mathbf{u}_i^* &= \mathbf{0}, \quad \text{on } \Gamma_u \qquad ,i = 1,2,3 \\ \mathbf{t}_i - \mathbf{t}_i^* &= \mathbf{0}, \quad \text{on } \Gamma_t \end{aligned} \tag{4.4}$$

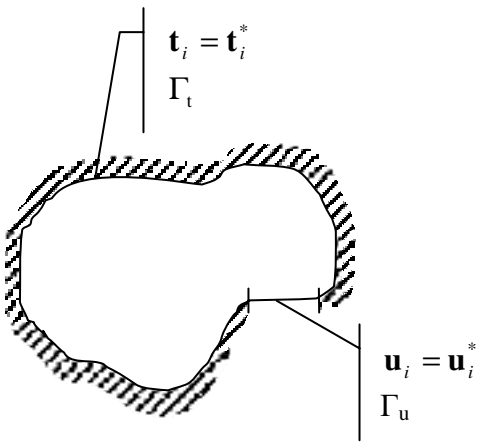

Fig.4.1 Domain for the state problem

4.2.2 Design Parameterization

We are interested in determining the optimal distribution of the given material in the design domain, i.e. we want to determine which points in space that should be material points and which should be void points. In our design domain Ω we are seeking the optimal subset Ω^{mat} of material points

$$\begin{aligned} &\mathbf{E} = \rho\mathbf{E}^0 \\ &\rho = \begin{cases} 1 \text{ if } x \in \Omega^{mat} \\ 0 \text{ if } x \in \Omega \setminus \Omega^{mat} \end{cases} \\ &\int_\Omega \rho d\Omega = Vol(\Omega^{mat}) \le V \end{aligned} \tag{4.5}$$

where $\rho \in \{0, 1\}$ is the discrete design variable and $\mathbf{E}^0$ is the stiffness tensor for the given isotropic material. Here the last inequality expresses a limit, V, on the amount of material at our disposal, so that the objective function will be satisfied for a limited, fixed volume.

The most commonly used approach to solve this problem is to replace the integer ρ with continuous variables by allowing intermediate values, which then are penalized to direct the solution towards discrete 0-1 values. In linear elasticity, ρ can be seen as the material mass density distribution and is now a function of the position in the design domain, i.e. $\rho=\rho(\mathrm{x})$. The penalization can be made by using a penalized, proportional stiffness model

$$\begin{aligned} &\mathbf{E}(x) = \rho(x)^p \mathbf{E}^0, \quad p > 1 \\ &\int_\Omega \rho(x) d\Omega \le V; \qquad 0 \le \rho(\mathrm{x}) \le 1, \quad \mathrm{x} \in \Omega \end{aligned} \tag{4.6}$$

One refers to ρ as the density of the material by the fact that the volume of the structure is evaluated as

$$\int_\Omega \rho(x) d\Omega \le V \tag{4.7}$$

The density interpolates the stiffness between the material properties $\mathbf{0}$ and $\mathbf{E}^0$;

$$\mathbf{E}(\rho = 0) = \mathbf{0} \text{ and } \mathbf{E}(\rho = 1) = \mathbf{E}^0 \tag{4.8}$$

4.2.3 Minimum Compliance Design

The objective of topology optimization is to determine a discrete valued design $\rho(x)$, which maximizes some efficiency measure, given by the objective function, subjected to one or more constraints. Here we want to solve a problem of topology design for maximum stiffness for a given structural weight. This problem is equivalent to design for minimum compliance defined as the work done by the set of given loads given the displacements at equilibrium, which in turn, is equivalent to minimizing the total elastic energy at the equilibrium state of structure.

4.2.4 Solution Methods

The method of solving a topology optimization problem starts by dividing the design domain into N finite elements. The stiffness E_e is discretized as constant in each element e =1,…, N. The state constraint then reads

$$\begin{aligned} &\mathbf{K}(\rho)\mathbf{u} = \mathbf{F} \\ &\mathbf{K} = \int_V \mathbf{B}^{\mathbf{T}}\mathbf{D}(\rho)\mathbf{B}dV \end{aligned} \tag{4.9}$$

where **u** is the nodal displacement vector, **F** is the load vector, **K** is the stiffness matrix, which depends on the design, and ρ is the design variable. Also **D** is the constitutive matrix and **B** is a constant matrix, giving the gradient of the shape function matrix. This relation implicitly defines the state variables, the displacements, as a function of the design variables, i.e. the material mass density ρ. The compliance can now be written as:

$$c(\rho) = \mathbf{F}^{\mathbf{T}}\mathbf{u}(\rho) = \mathbf{F}^{\mathbf{T}}\mathbf{K}(\rho)^{-1}\mathbf{F} \tag{4.10}$$

The finite element-discretized formulation of the topology optimization problem now reads:

$$\begin{aligned} &\text{objective function}: \quad \min c(\boldsymbol{\rho}) \\ &\text{constraints}: \quad \begin{cases} \mathbf{K}(\rho)\mathbf{u} = \mathbf{F} \\ \int_\Omega \rho \mathrm{d}\Omega \le V \\ 0 \le \rho_i \le 1, \end{cases} \end{aligned} \tag{4.11}$$

where V is the total available volume of materials.

The optimization is conducted through a numerical iteration process, which involves a first order mathematical programming algorithm. The Method of Moving Asymptotes (MMA) has proven to be well-suited for problems of topology optimization. The MMA works with a sequence of simpler approximate subproblems. The subproblems

are separable, convex and are constructed based on sensitivity information at the current iteration point as well as some iteration history. Asymptotes are introduced to stabilize the solution. They are dependent on the iteration history and are adjusted from one iteration to the next. In each iteration the compliance of the current design is computed, as well as the associated sensitivity with respect to design changes. This continues until only a marginal improvement in compliance is reached in the last design change.

A result of a 2D topology optimization is shown in the figures below. This simple problem shows a clip with forces applied to the gap of the clip, as well constraints that constrain certain nodes from displacement, marked by triangles in figure 4.2. The objective function is set to minimize the compliance, given that the displacement at nodes where that load is applied should not exceed a certain value. The topology optimization routine gives a framework solution, see figure 4.3.

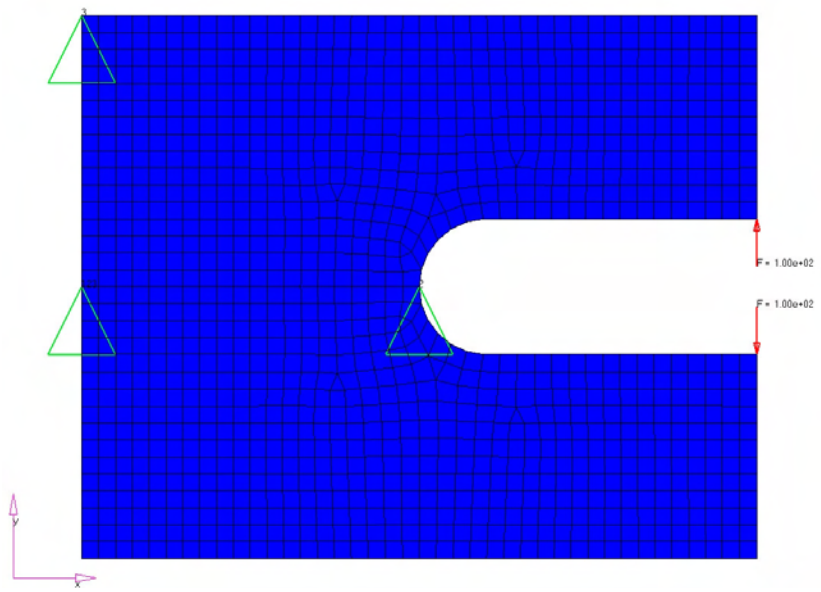

Fig.4.2 Topology optimization – problem set up of a 2D problem

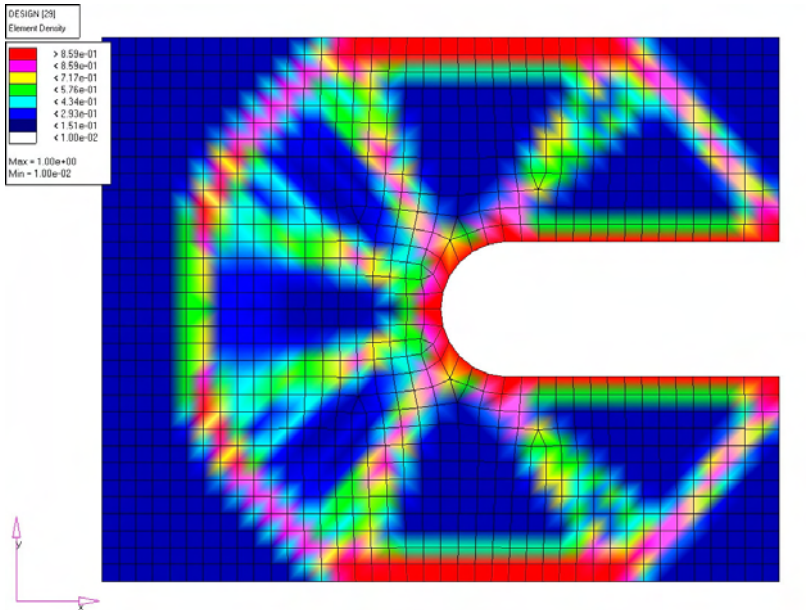

Fig. 4.3 Topology optimization – 1120 shell elements

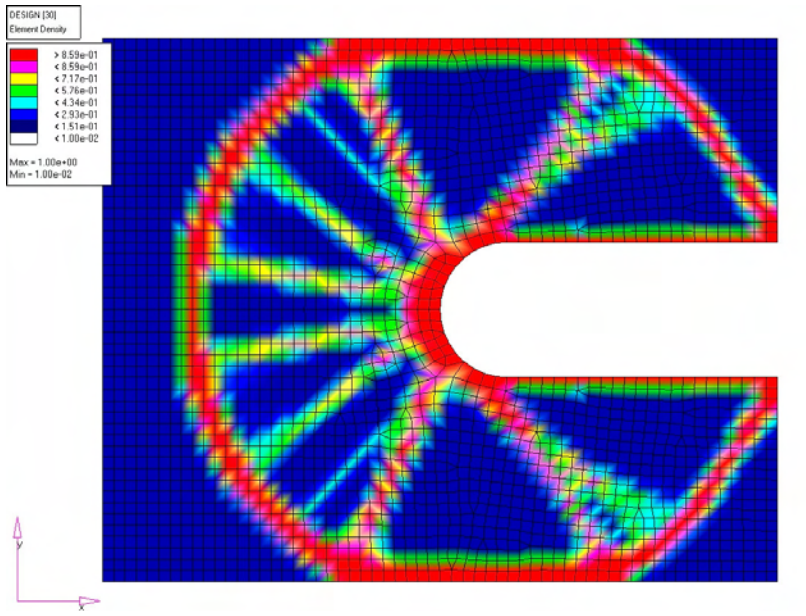

Fig. 4.4 Topology optimization – 2582 shell elements

4.2.5 Complications

There are two major numerical problems related to the solution of the topology optimization. These are the appearance of checkboards and the mesh-dependency of results. The former refers to the formation of regions of alternating solid and void elements, ordered in a checkboard like fashion. The problem is related to the discretization of the original continuous problem. Mesh-dependence concerns the effect that qualitatively different optimal solutions are reached for different mesh-

sizes or discretizations, see figure 4.3 and 4.4. The reason for mesh-dependency is that the penalized topology optimization problem in general lack a unique solution to converge to. This is due to the fact that the solution of the problem, given by feasible point $\mathbf{x}^*$ such that $f(\mathbf{x}) \geq f(\mathbf{x}^*)$ for all other $\mathbf{x}$, in general only can be met in a neighbourhood to $\mathbf{x}^*$.

One drawback with topology optimization is that it gives only a coarse layout of the boundaries of the structure. Shape and size optimization may be used for post-processing the result to determine the optimal final shape of the structure.

Chapter 5

Time Integration Methods

When solving a dynamic problem like the ones presented in chapter 3, time integration needs to be performed. There are two main types of integration methods, solved by either *explicit* or *implicit* algorithms. In this chapter these two algorithms will be briefly presented as well as their advantages and disadvantages.

5.1 Explicit Scheme

The FE discretization of the equations of motion is given by

$$\mathbf{M}\ddot{\mathbf{a}} + \boldsymbol{\psi}(\mathbf{a}) = 0 \tag{5.1}$$

where $\mathbf{M}$ is the mass matrix and $\boldsymbol{\psi}(\mathbf{a})$ the out of balance forces depending on the nodal displacement $\mathbf{a}$. A finite element formulation, like (5.1) contains a large number of nonlinear differential equations, which needs to be translated into algebraic equations in order to be solved iteratively. To do that, the Newmark time integration scheme may be used, given by

$$\mathbf{a}_{n+1} = \mathbf{a}_n + \Delta t\dot{\mathbf{a}}_n + \frac{\Delta t^2}{2}\left[(1-2\beta)\ddot{\mathbf{a}}_n + 2\beta\ddot{\mathbf{a}}_{n+1}\right] \tag{5.2}$$

$$\dot{\mathbf{a}}_{n+1} = \dot{\mathbf{a}}_n + \Delta t\left[(1-\gamma)\ddot{\mathbf{a}}_n + \gamma\ddot{\mathbf{a}}_{n+1}\right] \tag{5.3}$$

where β and γ are certain parameters and Δt is the time step. Different integration strategies are obtained depending on the particular choice of parameters. If $\gamma = \frac{1}{2}$ and $\beta = 0$, (5.2) and (5.3) can be written as

$$\mathbf{a}_{n+1} = \mathbf{a}_n + \Delta t \dot{\mathbf{a}}_n + \frac{\Delta t^2}{2} \ddot{\mathbf{a}}_n \tag{5.4}$$

$$\dot{\mathbf{a}}_{n+1} = \dot{\mathbf{a}}_n + \frac{\Delta t}{2} \left(\ddot{\mathbf{a}}_n + \ddot{\mathbf{a}}_{n+1} \right) \tag{5.5}$$

Using (5.4) and (5.5) it is straightforward to show that the equation of motion cf. (5.1) reduces to

$$\mathbf{M}\mathbf{a}_{n+1} = \mathbf{M}\left(2\mathbf{a}_n - \mathbf{a}_{n-1}\right) - \Delta t^2 \boldsymbol{\psi}\left(\mathbf{a}_n\right) \tag{5.6}$$

This algorithm is called the explicit algorithm. If the mass matrix is lumped, then (5.6) provides a set of uncoupled scalar equations. This is a great advantage of the explicit algorithm but it is not free from complications. To get accurate results from explicit time integration, the time step Δt must be limited. This is a constraint that must be fulfilled, otherwise the solution will be worthless. The time step is regulated by the speed of wave propagation within the material and the mesh. This implies that the time step must be so small that it affects all elements in the mesh. In some cases, in order to get a satisfactory mesh, there are a number of small elements concentrated to a certain area. To prevent these elements to set an unnecessary short time step a procedure called mass scaling might be used. This is done by increasing the density of these small elements so that the wave propagation becomes slower. It is important to carefully monitor these elements so that they do not corrupt the solution.

5.2 Implicit Scheme

When solving nonlinear equations with an implicit algorithm, the most widely used method is to linearise the equation at a given point, x_0, and then search for the state wanted. The solution given is not necessarily the correct solution, and therefore the procedure is repeated until the correct solution is located. For a simple one variable problem this approach may be visualised according to figure 5.1.

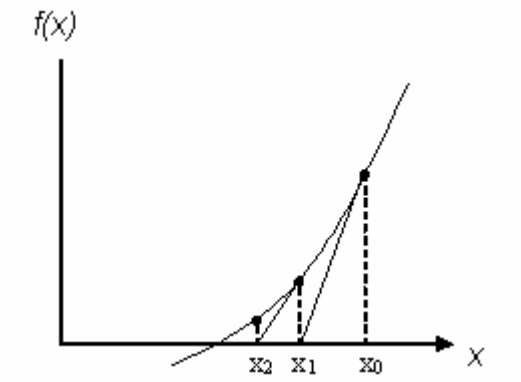

Fig 5.1 Implicit time integration

When deriving this method a different choice of the parameters β and γ is done. It will be assumed that β differs from zero. From (5.2) the following equation arises

$$\ddot{\mathbf{a}}_{n+1} = \frac{1}{\beta \Delta t^2}\left(\mathbf{a}_{n+1} - \mathbf{a}_n\right) - \frac{1}{\beta \Delta t}\dot{\mathbf{a}}_n - \frac{1-2\beta}{2\beta}\ddot{\mathbf{a}}_n \tag{5.7}$$

where all quantities are assumed to be known at a certain time t_n. The equation of motion at time t_{n+1} can be written as

$$\mathbf{M}\ddot{\mathbf{a}}_{n+1} + \boldsymbol{\psi}\left(\mathbf{a}_{n+1}\right) = 0 \tag{5.8}$$

Inserting (5.7) into (5.8) gives

$$\boldsymbol{\upsilon}\left(\mathbf{a}_{n+1}\right) = 0 \tag{5.9}$$

where ***v*** is a column matrix given by

$$\mathbf{v}\left(\mathbf{a}_{n+1}\right) = \mathbf{M}\left[\frac{1}{\beta \Delta t^2}\left(\mathbf{a}_{n+1} - \mathbf{a}_n\right) - \frac{1}{\beta \Delta t}\dot{\mathbf{a}}_n - \frac{1-2\beta}{2\beta}\ddot{\mathbf{a}}_n\right] + \boldsymbol{\psi}\left(\mathbf{a}_{n+1}\right) \tag{5.10}$$

Given that all quantities at the state n are known, it is possible to derive an iteration scheme using a truncated Taylor expansion of (5.10) according to

$$\mathbf{v}\left(\mathbf{a}^{i+1}\right) = \mathbf{v}\left(\mathbf{a}^{i}\right) + d\mathbf{v}\left(\mathbf{a}^{i}\right) \tag{5.11}$$

It will be assumed that $\mathbf{v}\left(\mathbf{a}^{i+1}\right)$ is zero, the differentiation of ***v*** may be written as

$$d\mathbf{v}\left(\mathbf{a}^{i}\right)=\mathbf{a}^{i-1}-\left[\left(\frac{\mathbf{M}}{\beta\Delta t^{2}}d\mathbf{a}+\int_{V}\mathbf{H}^{T}\mathbf{R}\mathbf{H}d\mathbf{V}d\mathbf{a}+\int_{V}\mathbf{B}^{T}\mathbf{D}^{t}\mathbf{B}dV\right)^{i-1}\right]^{-1}\mathbf{v}\left(\mathbf{a}^{i-1}\right) \qquad (5.12)$$

were **H** and **R** are certain matrices and $\mathbf{D}^{t}$ is the tangential constitutive matrix. For more information see Ottosen and Ristinmaa [3].

The displacement of the next iteration may now be established using (5.6) according to

$$\mathbf{a}^{i}=\mathbf{a}^{i-1}-\left[\left(\frac{\mathbf{M}}{\beta\Delta t^{2}}+\int_{V}\mathbf{H}^{T}\mathbf{R}\mathbf{H}dV+\int_{V}\mathbf{B}^{T}\mathbf{D}^{t}\mathbf{B}dV\right)^{i-1}\right]^{-1}\mathbf{v}\left(\mathbf{a}^{i-1}\right) \qquad (5.13)$$

As (5.13) shows, calculating the correction of the displacement involve inverting a matrix which requires a lot of computer power. The benefit with the implicit method compared to the explicit method is that the constraint of the time step is not as controlled as it is using an explicit scheme. Therefore the implicit algorithm suits problems with long load duration.

Chapter 6

Method Overview

The outline of the project is visualised through a flowchart, see figure below. Each step in the process is described in detail in the following chapters.

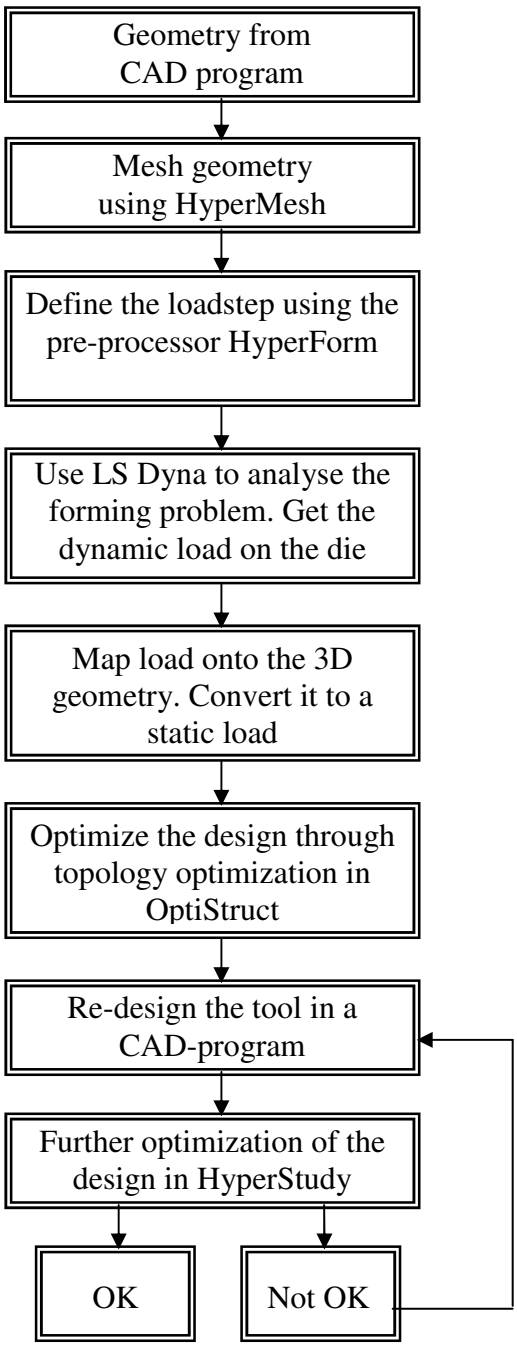

Fig. 6.1 Flowchart of project outline

Chapter 7

Geometry

The geometry files of the die, punch, blankholder and blank are delivered from VCBC, see figure 7.1. The original die is being considered but results can be attained for any other part of the stamping tool by analogous use the method described in this thesis.

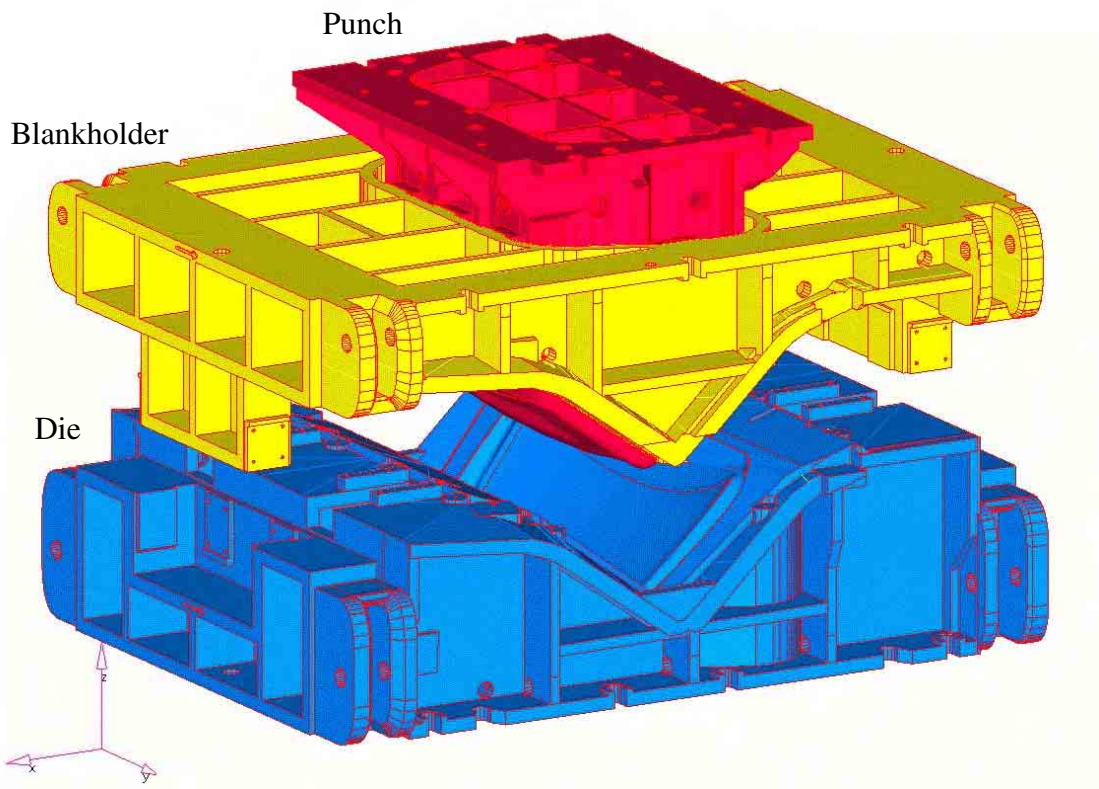

Fig. 7.1 Stamping tool of Volvo S80 trucklid

To prevent unnecessary problems, when in the future creating the mesh, a geometry clean up of the die is made. Details on the surface that are of minor interests in the simulation are eliminated in agreement with VCBC. These alterations can be seen in the figures below.

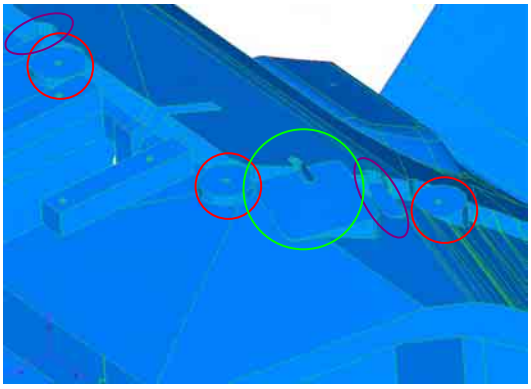

Fig. 7.2a Original model

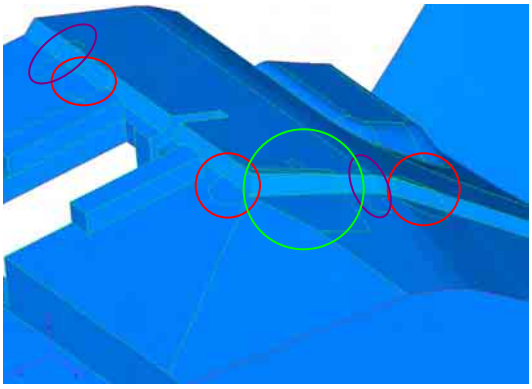

Fig. 7.2b Cleanup model

To get a perception of the die tool, different views of the original die are presented in the figures below.

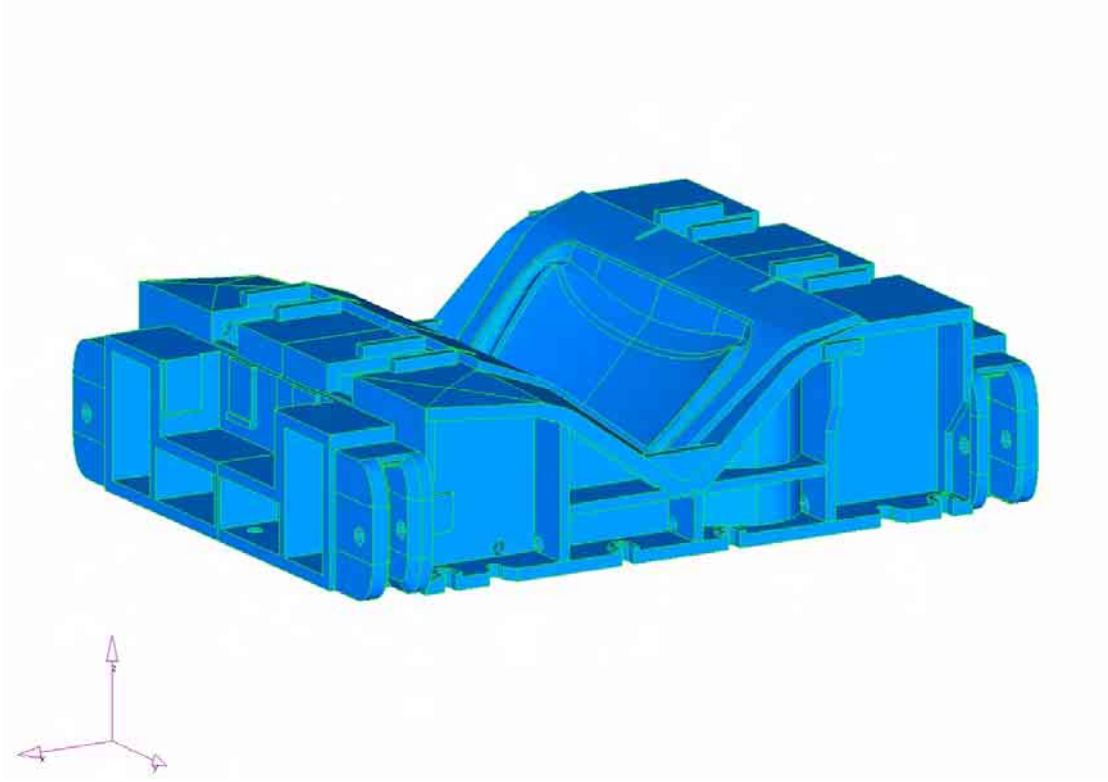

Fig.7.3a Isometric view of the original die

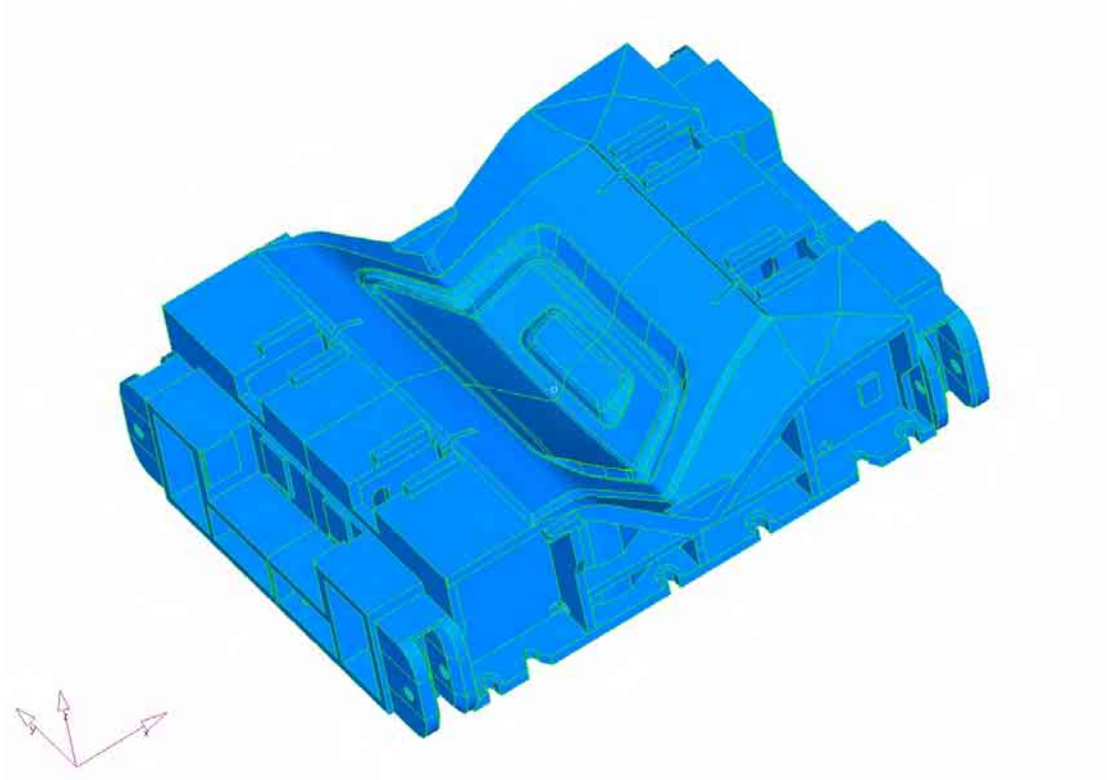

Fig. 7.3b Top/side view of the original die

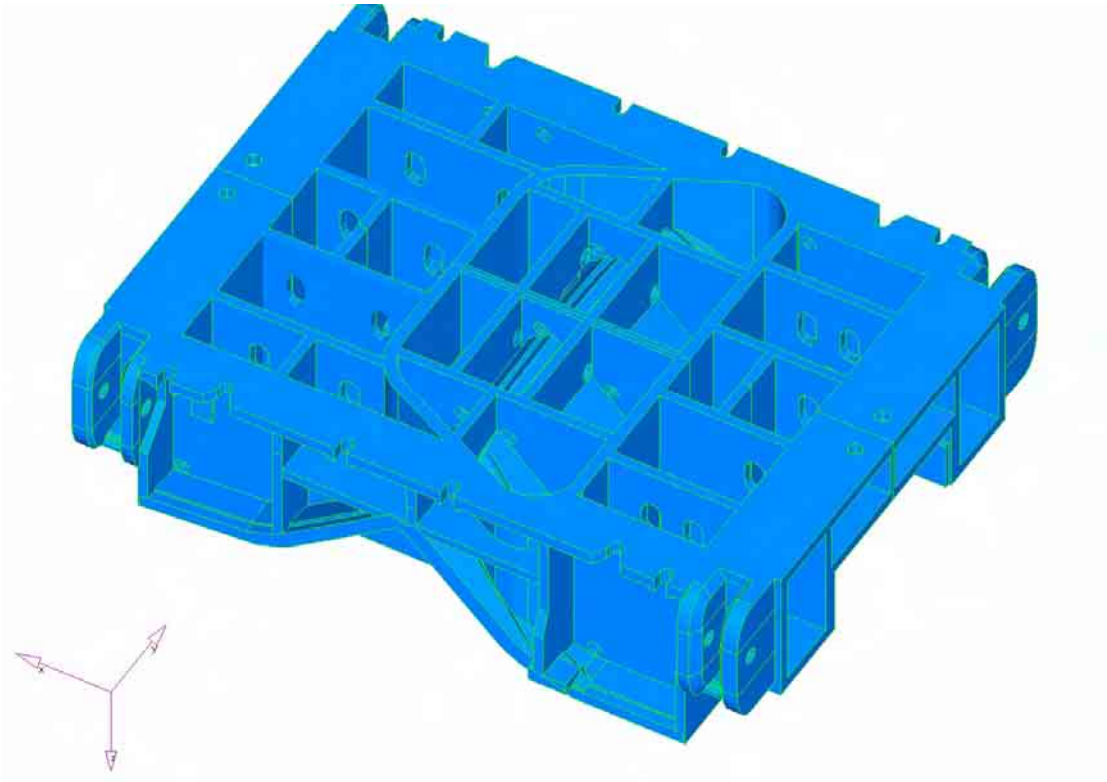

Fig 7.3c Bottom/side view of the original die

Chapter 8

Sheet Metal Forming Simulation

The loads acting on the die need to be known in order to be able to perform a topology optimization. The loads from the manufacturing process are obtained through a sheet forming simulation. A finite element model is created from the CAD geometry of the tool, which, although containing some simplification, still gives a very good approximation of the actual tool.

8.1 Model Description

The FE-model consists of the same parts as the original tool. However, the punch, blankholder and die are approximated to be rigid, and therefore only the surfaces in contact with the blank are needed in the FE-model, see figure 8.1.

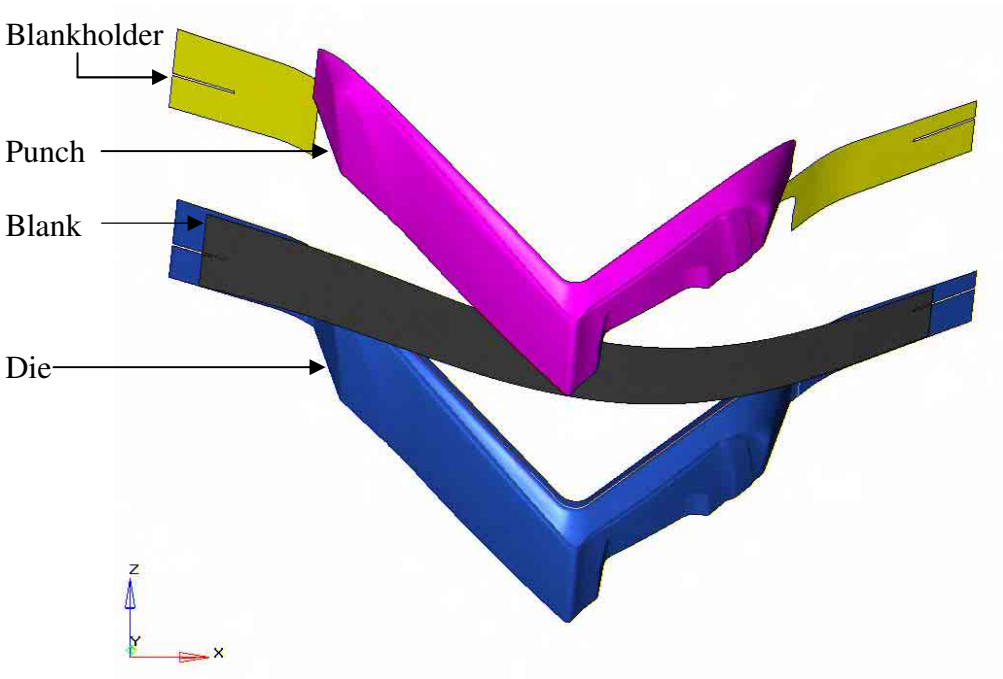

Fig. 8.1 FE-model of the forming process

In the model, a gravity force is applied to the blank, as well as a friction force between the interacting parts. In agreement with VCBC, the friction coefficient is set

to $\mu = 0.06$. To reduce calculation time, the symmetry of the tool is made use of, and only half of it is considered.

A nonlinear analysis must be performed, since the blank is subjected to large strains. Also because the load on the blank and contact between interacting parts are changed in every time step. To solve this dynamic problem, time integration needs to be done.

In sheet metal forming, the impact time is short and the time step will therefore be very small to ensure accurate solution. The most suitable approach in this case is the explicit time integration, where many uncoupled equations are solved simultaneously. There are a number of commercial finite element codes available, of which we have chosen to use LS-Dyna version 970 [6]. To set up the simulation, the guidelines in *Input Parameters for Metal Forming Simulation using LS-Dyna* [7] were used.

8.2 Mesh

The mesh of the tool parts created for the simulation of forming process is a rigid shell mesh, which is an approximation of the original tool that is in fact deformable. This mesh has one purpose, to describe the surface of the die as accurate as possible. Therefore there are no quality restrictions on the elements, such as minimum angle or length. Instead there are strong restrictions on the tool mesh deviation from the CAD surfaces, e.g. chordal deviation and angle between elements. On the other hand, the mesh of the blank is, naturally, a deformable mesh with quality restrictions. Figures of these two different meshes can be seen below.

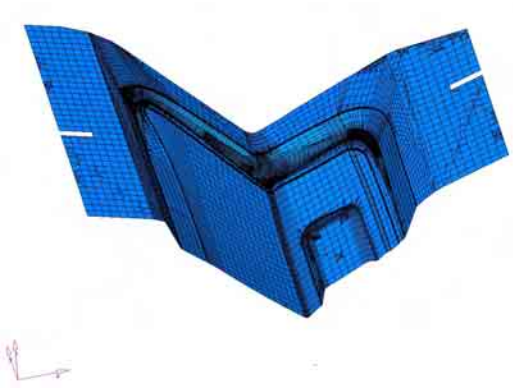

Fig.8.2a Rigid mesh of the die

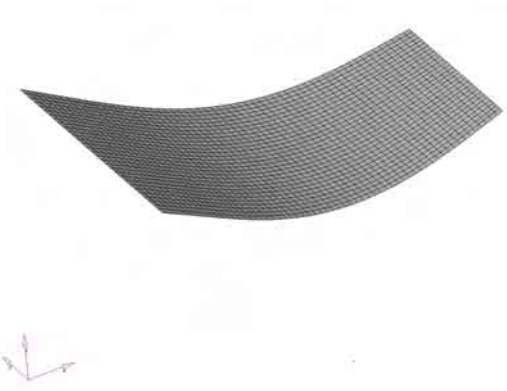

Fig.8.2b Mesh of the blank

8.3 Material Data and Material Model

As mentioned, all tool parts are modelled as rigid shell elements. The die is constrained in both displacement and rotation in all directions in the global coordinates, while the punch and blankholder are allowed to be translated in the z direction, see figure 8.1. The material data used for the tool is the parameters of steel

Density	$\rho = 7800$ kg/m^3
Young's modulus	E = 210 GPa
Poisson's ratio	$\nu = 0.30$

The Young's modulus and the Poisson's ratio are not needed in the explicit equations, because of the assumption of rigid tool. The values should however be realistic, since they are used in the contact definition and unrealistic values may cause numerical problems.

The blank is modelled as transversely anisotropic elastic-plastic material. This plasticity model is a generalization of the von Mises criterion to anisotropic materials, made by Hill. Plane stress is assumed and the input parameters needed are

Density	$\rho = 7800$ kg/m^3
Young's modulus	E = 210 GPa
Poisson's ratio	$\nu = 0.30$
Anisotropic hardening parameter	R = 1.78
Yield stress	σ_y =165 GPa

The yield function for Hill plasticity, assuming transverse anisotropy, is then given by

$$F(\sigma) = \left[\sigma_{11}^2 + \sigma_{22}^2 - \frac{2R}{R+1}\sigma_{11}\sigma_{22} + 2\frac{2R+1}{R+1}\sigma_{12}^2 \right]^{1/2} \tag{8.1}$$

where σ_{11} and σ_{22} are the two nonzero normal stresses, σ_{12} is the in-plane shear stress and R is the anisotropic hardening parameter.

8.4 General Problem Set up

The objective of the forming simulation is to give an as accurate approximation of the real process as possible. To do this one wants to use as little computer power as possible, by reducing the total run time of the simulation. There are two factors that effect the run time of an explicit simulation, total time to terminate the process simulated and the time increment.

The elements used in the blank sheet are in LS Dyna called Belytschko-Lin-Tsay shell elements. These elements are based on a combined co-rotational and velocity-strain formulation. The efficiency of the elements is obtained from mathematical simplifications that result from these two kinematical assumptions. The co-rotational portion of the formulation avoids the complexities of nonlinear mechanics by embedding a coordinate system in the elements.

8.4.1 Time Step

In LS-Dyna the maximum length of time step is set by the speed of wave propagation of sound in the smallest element.

$$\Delta t = \frac{l_{\min}}{c} = \frac{l_{\min}}{\sqrt{\frac{E}{\rho}}} \qquad \text{, where} \begin{cases} \Delta \mathrm{t} = \text{time step}, [\mathrm{s}] \\ \mathrm{l}_{\min} = \text{minimum element length}, [\mathrm{m}] \\ \mathrm{c} = \text{speed of sound}, [\mathrm{m/s}] \\ \mathrm{E} = \text{Young's modulus}, [\mathrm{N/m^2}] \\ \rho = \text{density}, [\mathrm{kg/m^3}] \end{cases} \tag{8.2}$$

If the time step is too large, the smallest elements are unaffected by the wave. Not to let these elements set an unwanted short time step, mass scaling is used. However this method introduces artificial dynamic effects, which may corrupt the solution and therefore needs to be monitored closely.

When performing a forming simulation in LS-Dyna, the time step may be establish from the recommendation below, were cycles per millimetre are the number of explicit time steps taken per millimetre of tool motion.

$$\text{Time step size} = \frac{1}{\text{Max. tool velocity} * \text{ Cycles per millimetre}} \tag{8.3}$$

Note that this is a guidance for setting the parameter in forming simulation and that the physical condition in (8.2) still needs to be met.

8.4.2 Tool Velocity

The tool velocity in the simulation may be increased from the physical one, to a certain extent, still giving a satisfying approximation of the forming process. This will speed up the process and reduce the run time of the simulation. However, it cannot be speeded up infinitely since this introduces kinematics effects, such as inertial effects, which will change the physical appearance of the simulated process.
Also, the total run time of the simulation augments, when the tool velocity is increased and the number of cycles per millimetre is kept constant, since this will reduce the time step, see equation (8.1) above. A well-adjusted balance of maximum tool velocity and the number of cycles per millimetre will give the shortest run time of the simulation.

8.4.3 Time Step Used in Forming Simulation of Volvo S80 Truck lid

The recommendation used in this thesis state that a value of between 100 and 1000 cycles per millimetre is recommended to give a reasonable time step. In accordance with VCBC, the parameter is set to 500. The recommended maximum tool velocity is 2000 mm/s, and to start and end the simulation with zero velocity. A simple trapezoidal velocity profile is used, see figure 8.3.

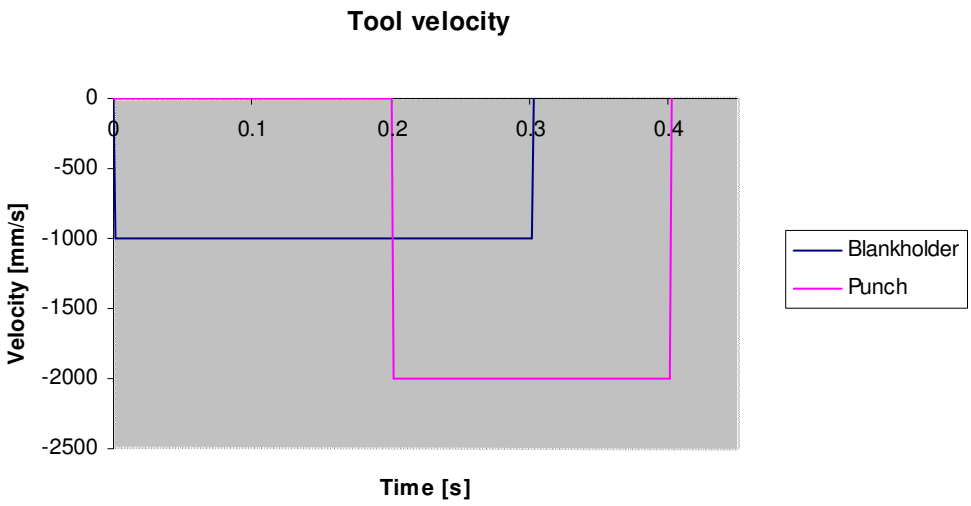

Fig. 8.3 Trapezoidal punch and blankholder velocity

For stability reasons a scale factor of 0.9 is used with the time step size parameter, giving a time step of 0.9 μs and the total time of the simulation is 0.4 s.

Minimum element length	$l_{min} = 0.005$ m
Speed of sound in steel	$c = 5170$ m/s
Maximum tool speed	$v_{tool} = 2000$ mm/s
Cycles per millimetre	$s = 500$ mm^{-1}

$$\left.\begin{aligned} \Delta t_{phys} &= \frac{0.005}{5170} = 0.967\mu s \\ \Delta t_{form} &= 0.9 * \frac{1}{2000 * 500} = 0.9\mu s \end{aligned}\right\} \quad \Delta t_{phys} > \Delta t_{form} \Rightarrow OK!$$

Our time step is smaller than the maximum time step defined to avoid mass scaling, that is, in our case, no mass scaling occurs.

8.4.4 Contacts

In metal forming simulations the contact between interfacing surfaces can be modelled by using a penalty method. This penalisation reduces any residual between to two surfaces that are to be in contact, by multiply it by some penalty factor, which thereby works like a spring in-between the two surfaces. A “forming-one-way” type of contact is recommended. This interface computes tooling curvature information in every time step, used to determine if an adaptation refinement is needed (see next section). In order to avoid undesired oscillation in the contact, a constant damping perpendicular to the contacting surfaces is applied.

8.4.5 Adaptivity

Adaptivity is applied to the blank mesh to obtain the greatest accuracy for the given set of computational resources. In the initial mesh, the elements with the largest error indicator are subdivided into smaller elements. In our case, an increased error indicator is defined by either a large angle between two elements or by the blank getting closer to a tool part that demands smaller elements. The free nodes in the new elements are constrained to move as the average value of the neighbouring original nodes displacements. Adaptivity does not provide control on the error of the solution, but it makes it possible to obtain a solution of comparable accuracy with fewer elements, than with a fixed mesh. The adaptive process can consist of several refinement levels, see figure 8.4. Each refinement might cause mass scaling, since it may generate a new smallest element.

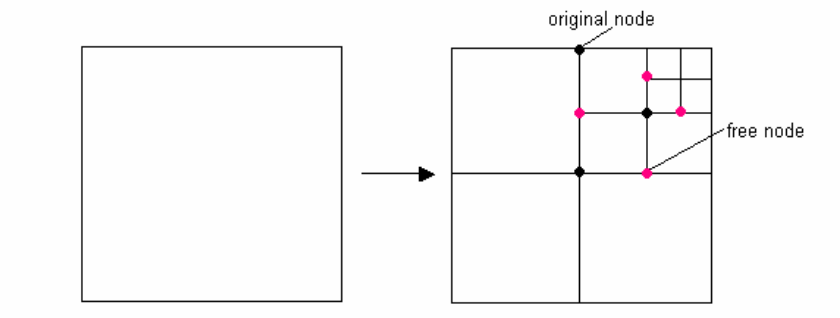

Fig. 8.4a Initial element size *Fig.8.4b* Mesh after three refinement levels

8.4.6 Drawbeads

In the actual metal forming process there are drawbeads around the cavity of the die, to help control the forming of the blank. These are simulated as analytic drawbeads, defined by a set of node points that create a line on the die surface, see figure 8.5. Along the drawbead line both lifting and friction force are applied, which serves as an approximation of the actual drawbead.

Fig. 8.5 Die with analytic drawbeads (red line)

8.5 Forming Simulation of Volvo S80 Truck lid

The problem set up starts with an implicit gravity analysis of the sheet. In implicit analysis, equilibrium of the FE-equations is established in each time step. The sheet is very thin in the direction of the gravity in comparison with the two other directions, and density of the material is high. This causes large deflection from the original horizontal position, see figure 8.6.

Fig. 8.6 Deformation due to gravity load

The simulation of the actual forming process is performed as a so-called multi-forming simulation, which starts by the blankholder closing and fixating the blank to the die. Halfway through the blankholder motion, the punch motion starts, see figure 8.7a and 8.7b. Analytical drawbeads are applied to the die, to help give the blank the required final shape.

Fig. 8.7a Set up of forming simulation – start position

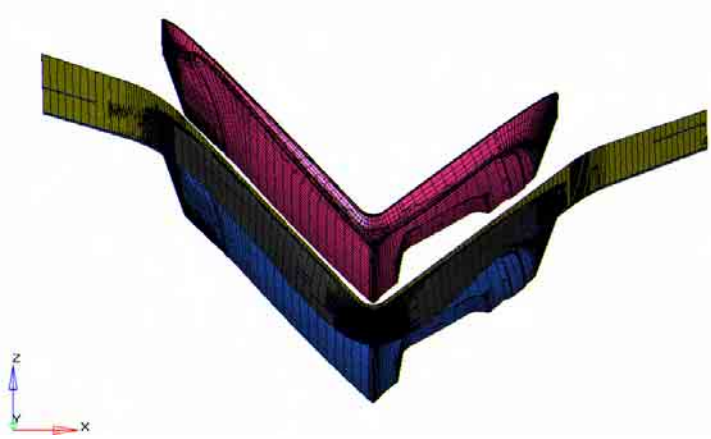

Fig. 8.7b Set up of forming simulation – blankholder closed

The set up of the forming simulation proved to be more complicated and time-consuming than expected, due to coarse set forming parameters in LS-Dyna. We also had some trouble retaining satisfactory result from the forming simulation. Non-optimal CAD-geometry lead to unrealistic contact pressure, at a maximal value of 240 MPa, between the die and the blank under the influence of the blankholder force. Once this was corrected, better but still not satisfying blankholder pressure was attained due to incorrect tool offset in this area. As a result, the contact pressure caused by the blankholder needed to be manually altered go give a realistic approximation of the forming process and the normal contact pressure were uniformly set to 3 MPa.

The result of our forming simulation can be seen in figure 8.8, where the adaptivity of the mesh is clearly seen. The outer material of the final shape is waste material, needed in the forming process to fixate the blank. This material will later be removed.

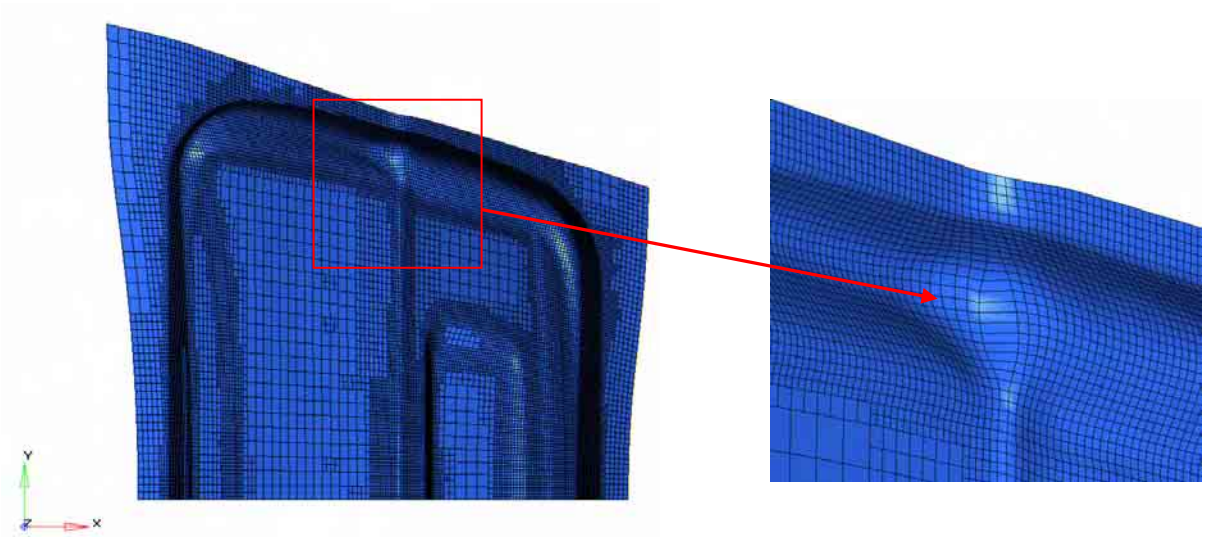

Fig.8.8 Final shape of deformed blank

As demonstrated in the right part of figure 8.8, we get some torn elements in the knee of the blank. This can also be seen in the FLD (see chapter 2) of the forming process, in figure 8.9. The input parameters for the FLD is the blank thickness, t = 0.77 mm, and the strain-hardening exponent, n = 0.229.

An attempt was made to improve simulation, using a different tool offset and some other LS-Dyna input parameters, see Appendix A. However, this did not give significant better result. Naturally, this is not a good enough approximation and further efforts needs to be made in the future.

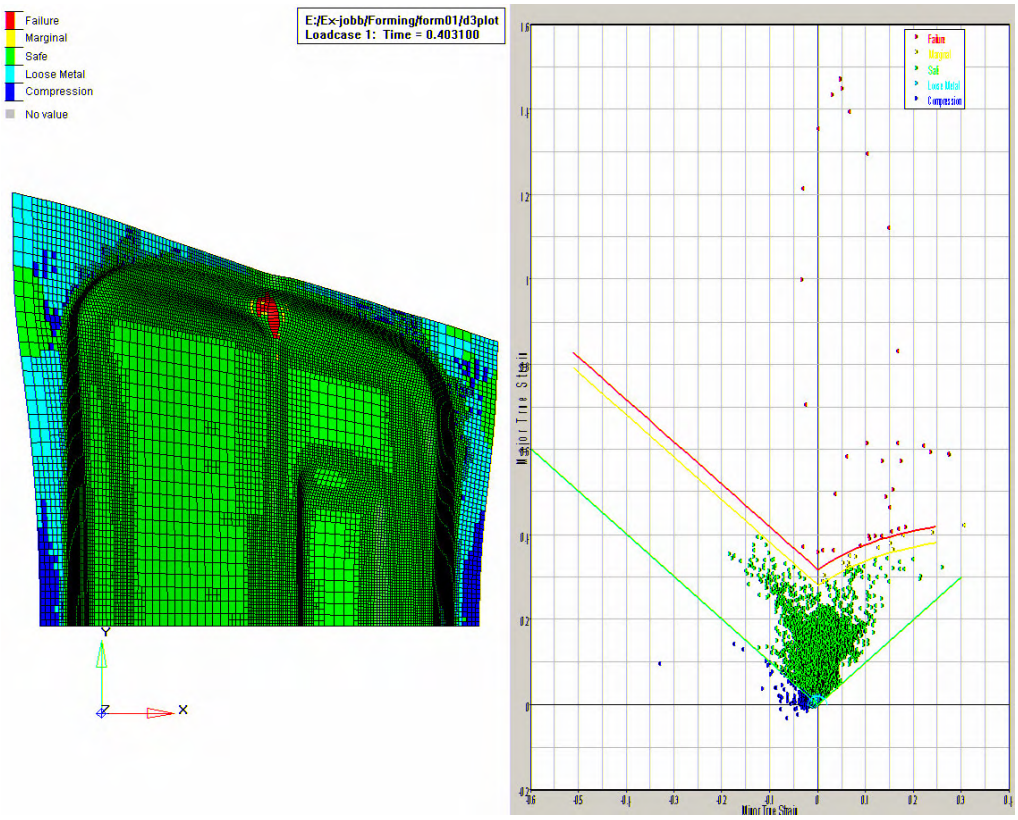

Fig. 8.9 FLD diagram of the final shape of deformed blank,
n = 0.229 and t = 0.77

Chapter 9

Topology Optimization

The loads on the die from the forming process were attained in the previous chapter. In order to make a topology optimization, the constraints on the die needs to be defined as well. Once a proper problem set up is established, a quasi-static topology optimization is performed, to determine the optimal material distribution within the design domain. In order to solve the topology optimization problem, the finite element software HyperMesh is utilized to prepare the problem set up, and the linear solver OptiStruct is used to obtain the optimal material distribution.

9.1 Model Description

The geometry of the die tool structure is modelled by the use of 3D solid elements. Since one of the objectives in this project is to find the optimal material distribution in the die tool, without changing the current design of the Volvo S80 truck lid, the material in contact with the blank in the forming process are set as a non-design space. That is, the characteristic of this material is not to be changed during the topology optimization. For VCBC to be able to use the same press in manufacturing, the outer shape of the die is also set as non-design space. To enable the topology optimization to find the optimal distribution of material, the entire volume underneath the non-design space is set as available design space, see fig 9.1. The non-design space is the red area in the figure, which is to be maintained during the topology optimization. The green space, on the other hand, is the defined design space, which will be optimized.

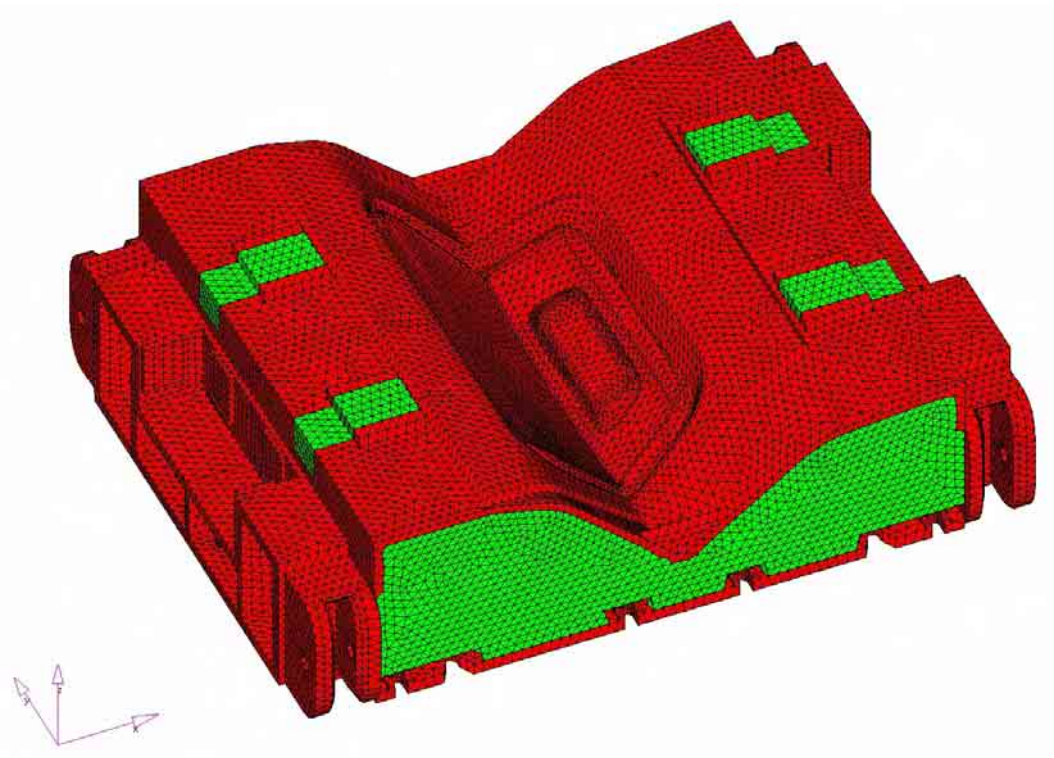

Fig. 9.1 FE-model used for topology optimization

9.2 Mesh

The mesh used for topology optimization is a solid element mesh. The solid element types considered for this project were hexahedron and tetrahedron elements. For the interested reader, these elements are in OptiStruct called CHEXA and CTETRA, respectively. Hexahedron elements are elements with six sides and eight nodes. Tetrahedron elements are elements with four sides and four nodes. Figures of these two different types of elements can be seen below.

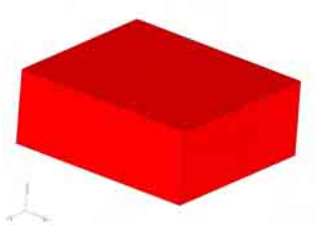

Fig. 9.2a Hexahedron element

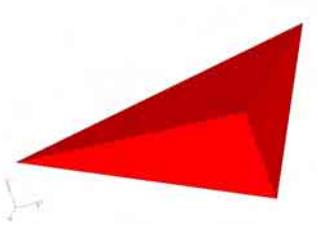

Fig. 9.2b Tetrahedron element

Before we started the assigned project, we practiced the problem set up on a small model. We tried both hexahedron and tetrahedron mesh on this test model. We found that the results from

the topology optimization were similar, but also that the processing time was approximately 2.5 hours with the tetrahedron mesh and 8 hours with the hexahedron mesh. A hexahedron mesh is also a time consuming mesh to set up in comparison with a tetrahedron mesh. Given that the results were similar and the processing time were noticeable shorter when using tetrahedron mesh, we decided to use this type of element for our topology optimization. The mesh generated for the die tool to be optimized can be seen in fig 9.1.

9.3 Material Data and Material Model

After the mesh is defined, material properties must be assigned to the elements. In our case, the material law used defines the properties for a linear, temperature-independent, isotropic material. The material data is given by the same parameters as has been used earlier for the die, see section 8.3. Note that since the material is homogenous, the magnitude of the input parameters is of no importance, as long as the ratio between them is constant.

9.4 General Problem Set up

In the set up of a topology optimization problem, the total package volume needs to be divided into a design and a non-design space, according to the restrictions of the problem. Also, at least one load case, with associated boundary conditions, need to be defined.

The earlier defined design space is set to be the domain to be optimized, thereby defining the design variables as the elements of this domain. The optimization is conducted for the given objective function, for example to minimize the compliance, of the problem. Constraints needs to be applied as well, or the otherwise obtained solution would be the full design space, which naturally provides the stiffest solution.

A concern in topology optimization is that the design concept developed is often not manufacturable. To satisfy the casting conditions, minimum and maximum member size of the ribs created can be controlled, as well as the draw direction of the part. Another feature is pattern grouping that allows a part of the domain to be designed in a certain pattern, for example that two halves of the domain should be symmetrical.

9.5 Topology optimization of Volvo Die

The elements of the design space earlier defined are set as the design variables of the die tool. We have been given two load cases from VCBC, for which the die should be optimized. The first load case is attained from the forming simulation, where contact pressure and drawbead forces on the die are found. The loads are mapped from the LS-Dyna model to the FE-model of the topology optimization, by use of a modified Delaunay algorithm. The Delaunay algorithm maps node data from one coordinate system to the element at the same position in the other coordinate system. The element is then triangulated and the data from adjacent triangles are interpolated into a final mapped value. The mapping is made from the rigid shell mesh of the die tool, used in the forming simulation, to a deformable shell mesh, which represents the surface of the solid mesh established for topology optimization. After that, another mapping is performed, from the shell elements to the solid elements.

The second load case is the lifting of the die in the lifting lugs, an operation needed for transportation and cleaning. For safety reasons, the transportation of the tool will be considered as a slow movement and a safety factor of $\varphi = 1.1$ will be multiplied with the weight of the tool in accordance with Kran- och Hisskommissionen [8]. Both load cases are quasi-static, i.e. they are actually dynamic, time dependent loads that are approximated to be static load, needed in the topology optimization.

The boundary conditions applied to the forming load case is created by clamping the fixation hole on the bolster side of the die, in all displacement directions. The die is also prevented from moving in the vertical direction by locking the bed side from z displacement, see fig 9.3.

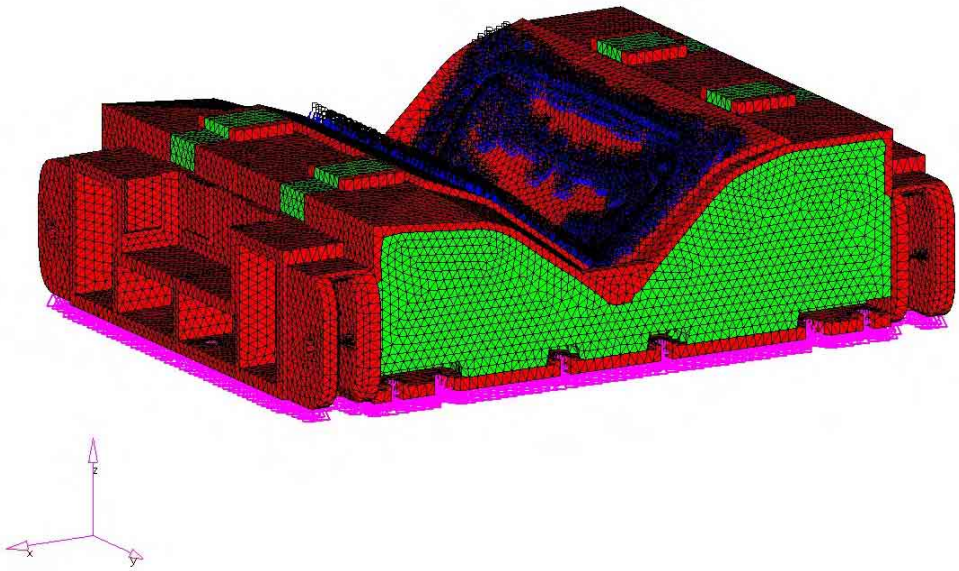

Fig. 9.3 FE-model of the forming load case for topology optimization

In the lifting load case, the nodes in the lifting lugs are constrained in all degrees of freedom except for the x-axis rotation, see fig 9.4

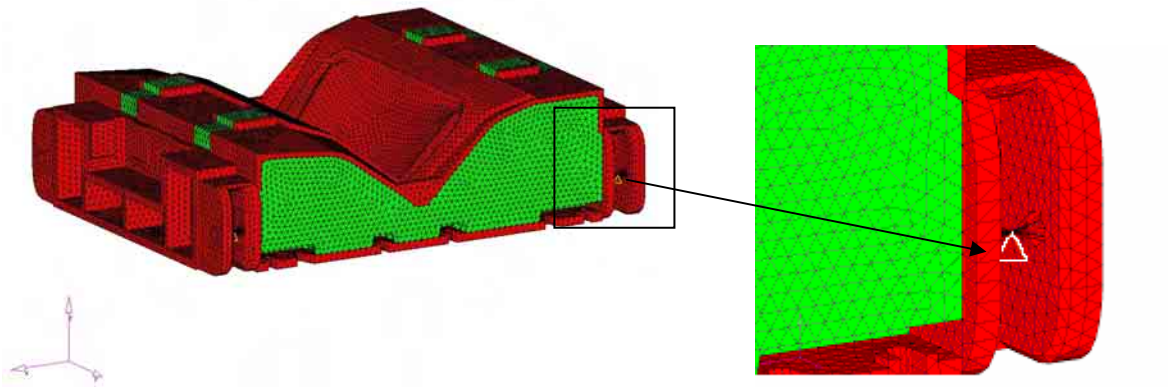

Fig. 9.4 FE-model of the lifting load case for topology optimization

In our set up of the topology optimization problem, the two load cases are weighted equally. The forming load case occurs to a much larger extent than the lifting case, however, as a safety precaution they are still given the same relevance. The objective function is set to find the minimum compliance, that is the maximum stiffness, of the package domain. The constraint is set to use only 15 % of the volume of the design space, by defining a volume fraction of 0.15. The result of this topology optimization can be seen in the next chapter.

One of the objectives of this thesis is to reduce the weight of the die, and to meet this demand we had to elaborate with different volume fractions. A volume fraction of 0.50 gave a coarse structure where ribs where hard to define, while a fraction of 0.30 gave clearer, but still not satisfactory results. Finally, a volume fracture of 0.15 was found to give a legible structure, see chapter 10 for details.

We also found that better results were achieved when the entire die was used in the topology optimization, instead of using only half of it, together with a symmetry plane. The symmetry plane caused a material distribution pattern that seemed to give element near this surface a higher priority.

Attempts were made to illustrate the non-rigid response of the press, by placing a layer of elastic material under the die. However, this bed seemed to distort the defined draw direction, giving a topology optimization result that was hard to interpret.

Also, we tried to determine the mesh dependency of the topology optimization problem by reduce the element size. This resulted in a very time consuming calculation, that gave a nonsense structure.

Chapter 10

Topology Optimization Results and Re-design of the Die

The results from the topology optimization can be viewed in fig 10.1 and 10.2. These are the results satisfying the objective function and the constraints, to minimize the compliance and to use a volume fraction of 0.15. It should be used as an indication of the new design of the die for this given load. The outer red frame in the figures is earlier set as non-design space and therefore they will remain fix through the topology optimization. The red areas in the design space indicate that the structure reaches the bolster of the die.

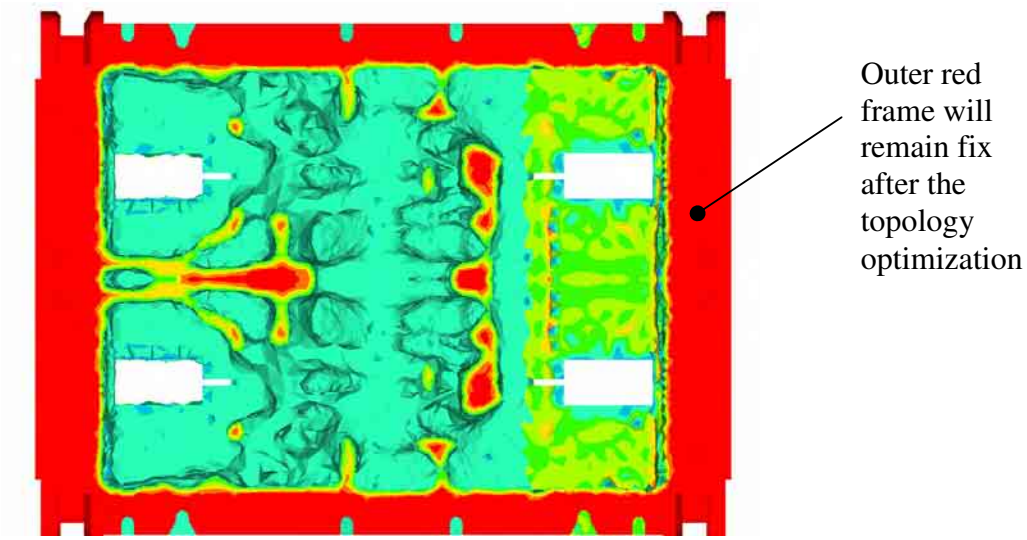

Fig 10.1 Results from the topology optimization of the die

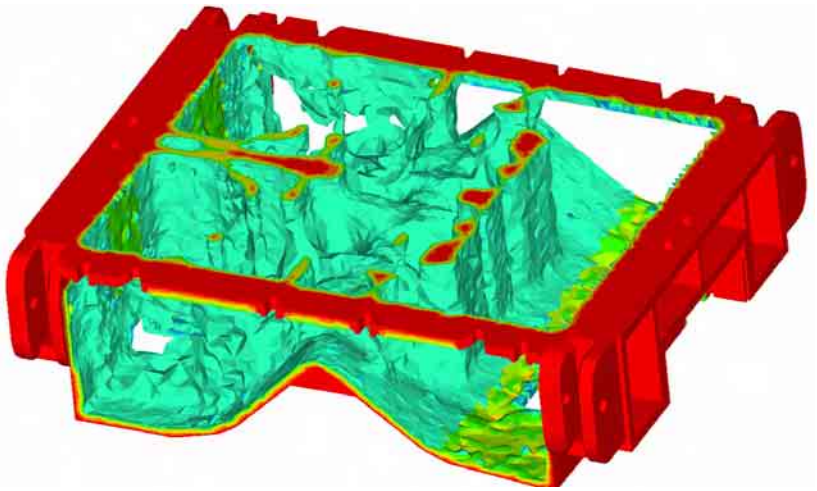

Fig 10.2 Results from the topology optimization of the die

10.1 Interpretation of the Result

Fig 10.3 shows our interpretation of the rib structure from the topology optimization. In the centre of the die is the spine, from which several ribs emerge. The ribs on each side of the spine are joined together by a transverse rib. On the left hand side, two symmetric V's are created, as well as two closing walls, which attach the top non-design surface to the bolster one. In the figure, broken lines illustrate that the ribs do not reach the bolster of the press.

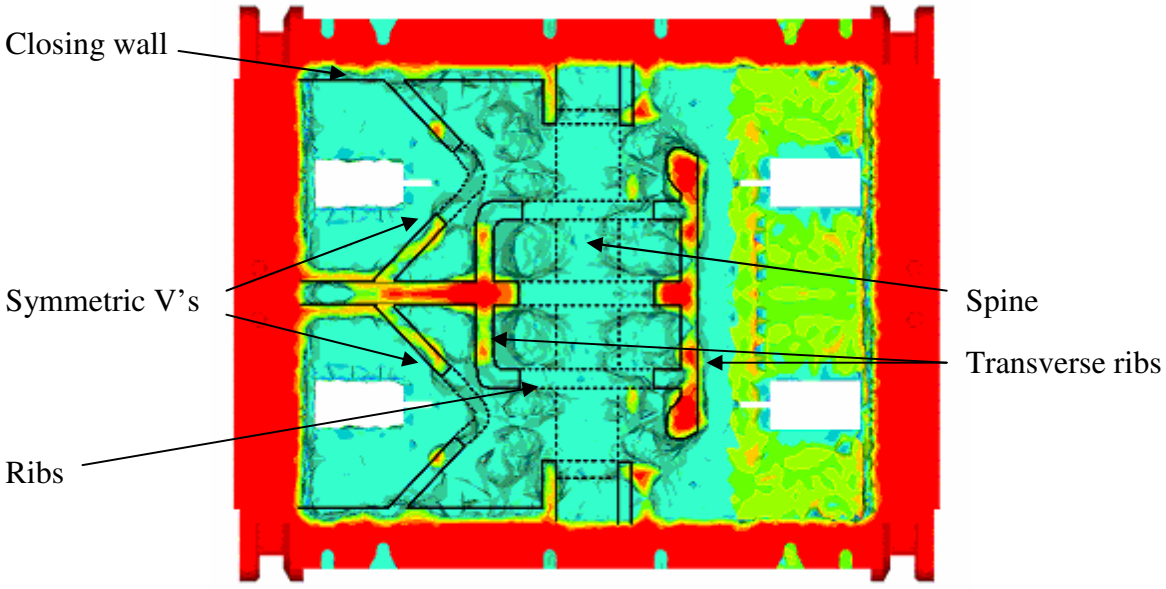

Fig 10.3 Our interpretation of the topology optimization results of the die

10.2 Re-design of the Die

A CAD-model is created from the pattern seen in the result of the topology optimization. The CAD-program used in this project is Solid Works 2006 [9]. The non-design surfaces are maintained, and are exported from HyperMesh into Solid Works. The new rib structure, shown in fig 10.3, is created. Fig 10.4 and 10.5 shows the CAD-model of the new, optimized die.

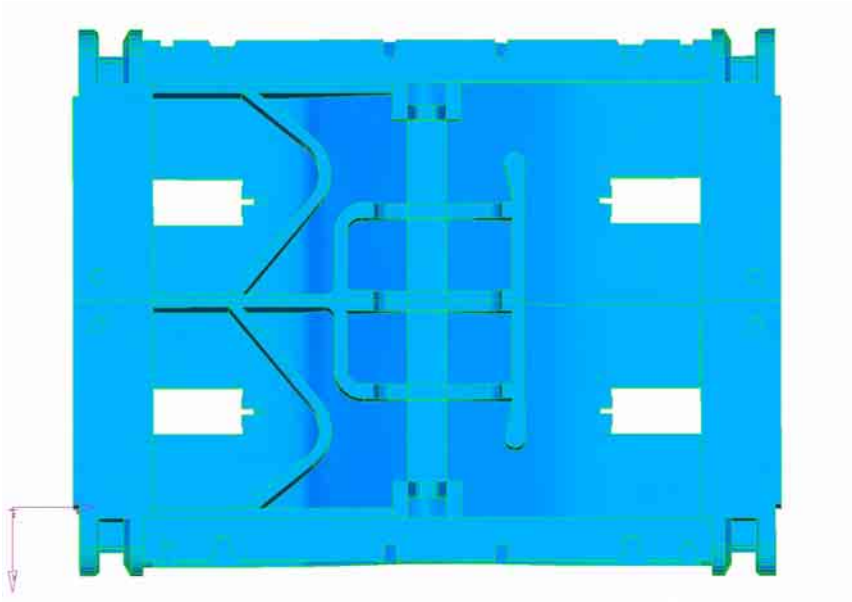

Fig 10.4 CAD-model of the new and optimized die

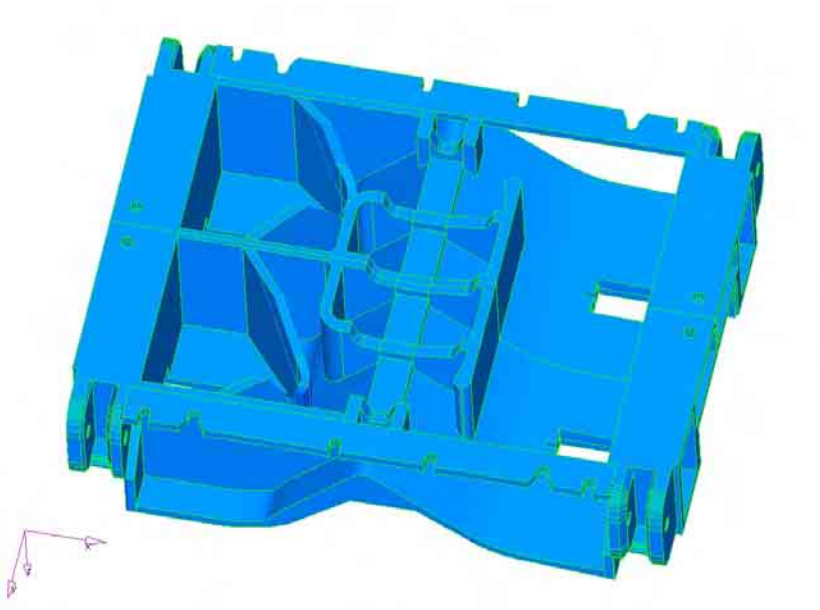

Fig 10.5 CAD-model of the new and optimized die

When evaluating the result, it is important to keep in mind that this is the result of an exact given load, and that variations in the applied load might give a different result. To get an indication of how stable our solution is, a load from a different forming simulation is applied on the die, and a topology optimization is performed. The results can be viewed in appendix A, fig A.2. This solution is slightly different but the overall structure is similar. Therefore we believe that our solution is sufficiently stable.

A great advantage with topology optimization is the fact that you will get the optimal design, irrespectively of the number of load cases applied. These load cases can be of great complexity and hard for the human mind to grasp. To get a better understanding of how the loads effect the result of the topology optimization in this project, we performed a topology optimization for each separate load case. Therefore, separations of the loads have been made and the normal pressure, shear forces, gravity forces and the drawbead forces have been applied, one at a time. These topology optimization results can be found in appendix B, fig B.1 till B.8, where it can be seen how the different load cases effect the overall solution. It is interesting to note that the spine pattern is the result of the normal pressure, and the closing walls are generated from the lifting case when transporting the tool.

Chapter 11

Displacement and Stress Analysis of Optimized Die

To analyse the results of the optimized die we look at the displacements and von Mises stresses in the die. As mentioned earlier, the die is subjected to a forming and a lifting load. The displacements and stresses are remarkably higher in the case of forming compared to the lifting case, and therefore we will focus on the results from the forming simulation in future discussion. These results will be compared with the displacements and von Mises stresses in the original die.

The CAD-model is used to set up a FE-model of tetrahedral elements. These elements are changed from first order into second order elements. Since second order tetrahedral elements have 10 nodes while first order tetrahedral elements have only 4 nodes, the surfaces will be better described. This will improve the accuracy of the result. Results and analyses of the displacements can be viewed in fig 11.1 till 11.4 and the stresses in fig 11.6 until 11.9. Table 11.1 shows the numerical values of the displacements, stresses and weight in the original and optimized die. The weight of the optimized die is 19% lighter than the original and the maximal displacement is 15% less the size of the original.

	Volvo Original Die	**Topology Optimized Die**	**Difference**
Maximal displacement (mm)	0.322	0.275	-15%
Maximal von Mises Stress (MPa)	106.1	140.3	+32%
Weight (kg)	9605	7826	-19%

Table 11.1 Comparison between original and optimized die

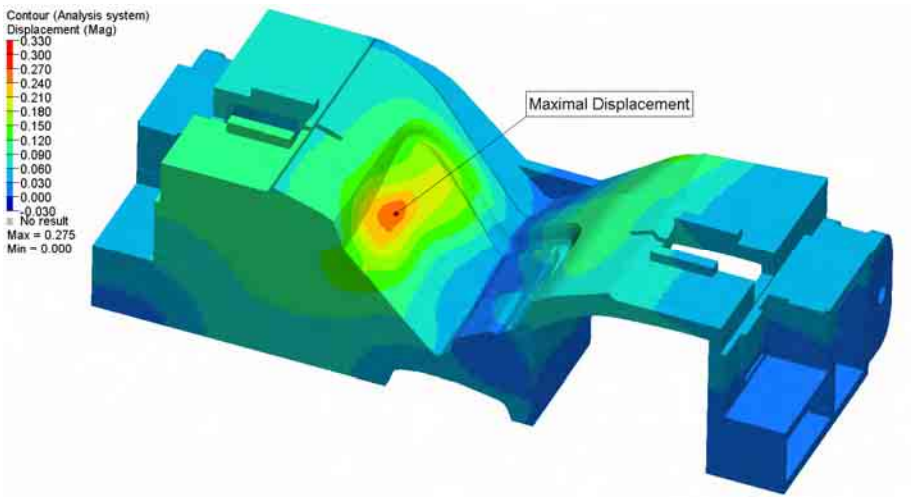

Fig 11.1 Displacement analysis of optimized die

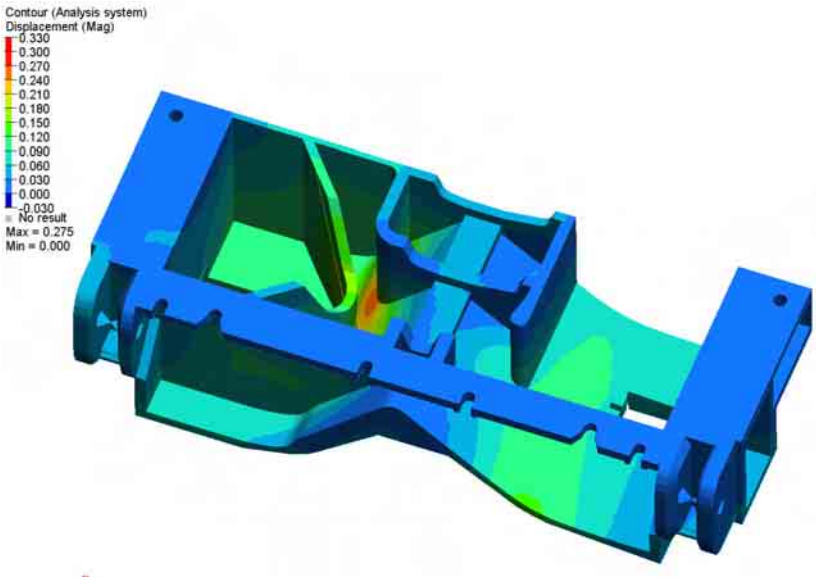

Fig 11.2 Displacement analysis of optimized die

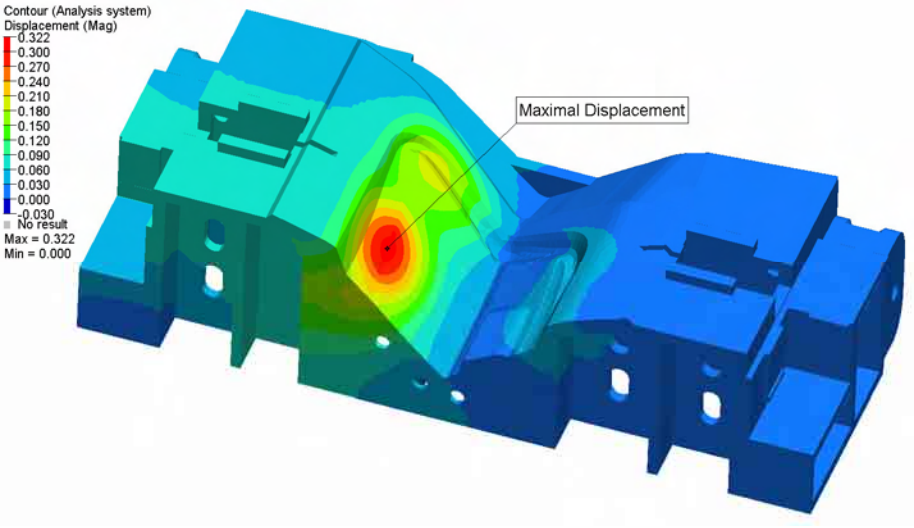

Fig 11.3 Displacement analysis of the Volvo die

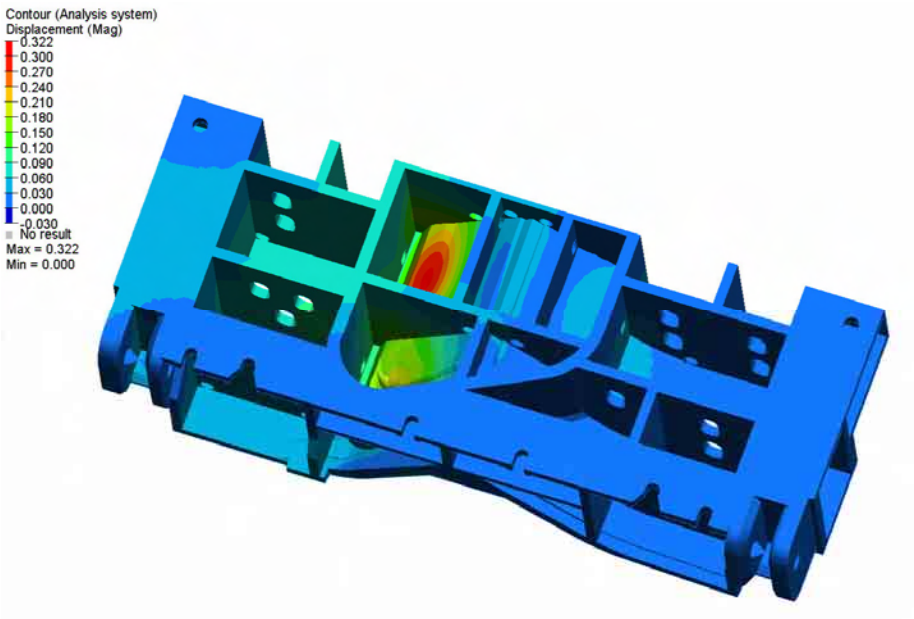

Fig 11.4 Displacement analysis of the Volvo die

11.1 Displacement Analysis

For the displacements to be comparable we need to consider their directions. Fig 11.5a and 11.5b marks the negative direction and magnitude of the displacements. Since they are approximately normal to the surface, both in the original die as well as the optimized die, they are comparable.

If we focus on the overall displacements, instead of the maximal displacements, we note that the right side of the die in fig 11.1 has lower stiffness than the same side of the VCBC die in fig 11.3. This is the result of there being less material and supporting ribs on this side. The reason for this is that in the topology optimization the limited material used is better needed on the other side, for this given load. Consideration should naturally be made that the design is sustainable for variation in applied load.

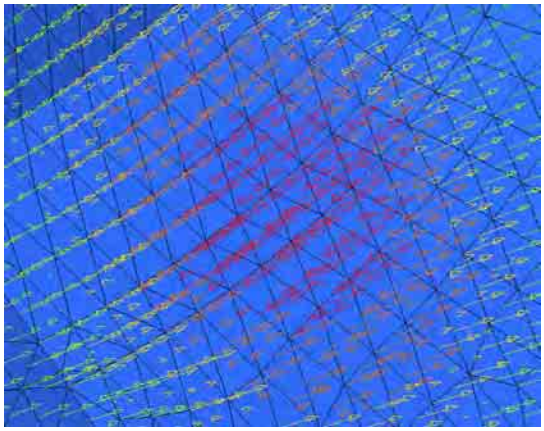

Fig 11.5a Magnitude and negative direction of displacements in original die

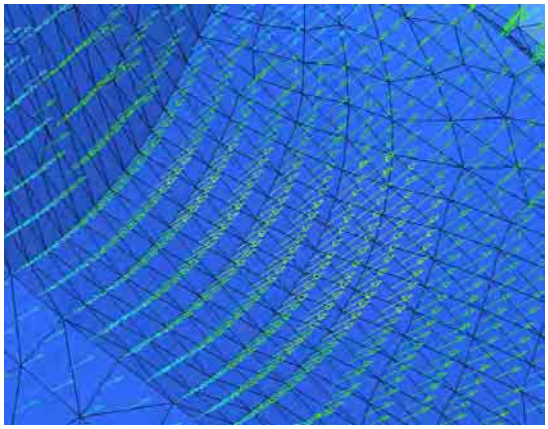

Fig 11. 5b Magnitude and negative direction of displacements in optimized die

11.2 Von Mises Stress Analysis

The result of the analyse of the von Mises stresses shows that the maximal stress in the optimized die is 140 MPa, and located on the surface of the die, as shown in fig 11.6. In a close up picture of the exposed area, it can be seen that these high stresses acts locally on one element. Since the surrounding elements are not nearly as exposed to high stresses, a discretisation error might have occurred, see fig 11.10 for details. This discretisation error may be caused by a defect in the mesh, as well as a numerical problem caused by the mapping procedure. Except for this local error, the overall stress distribution in the optimized die is comparable to the VCBC die.

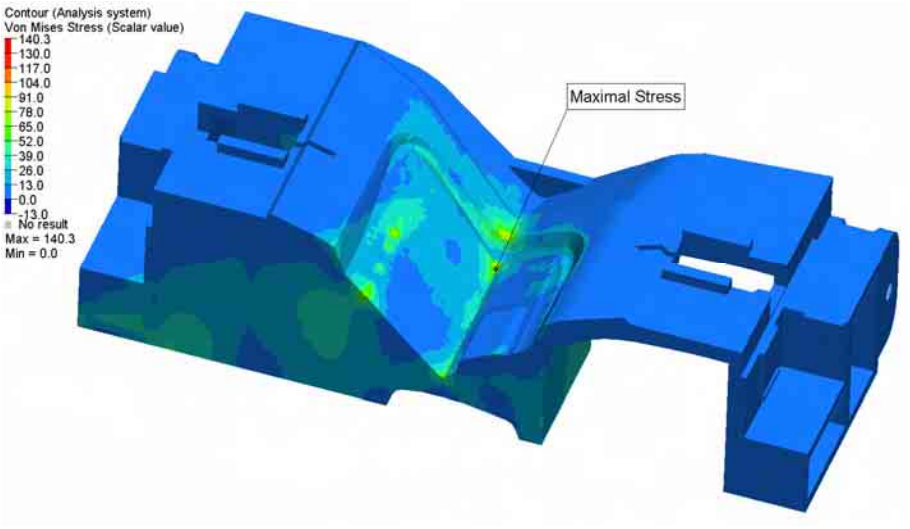

Fig 11.6 Von Mises Stress analysis of optimized die

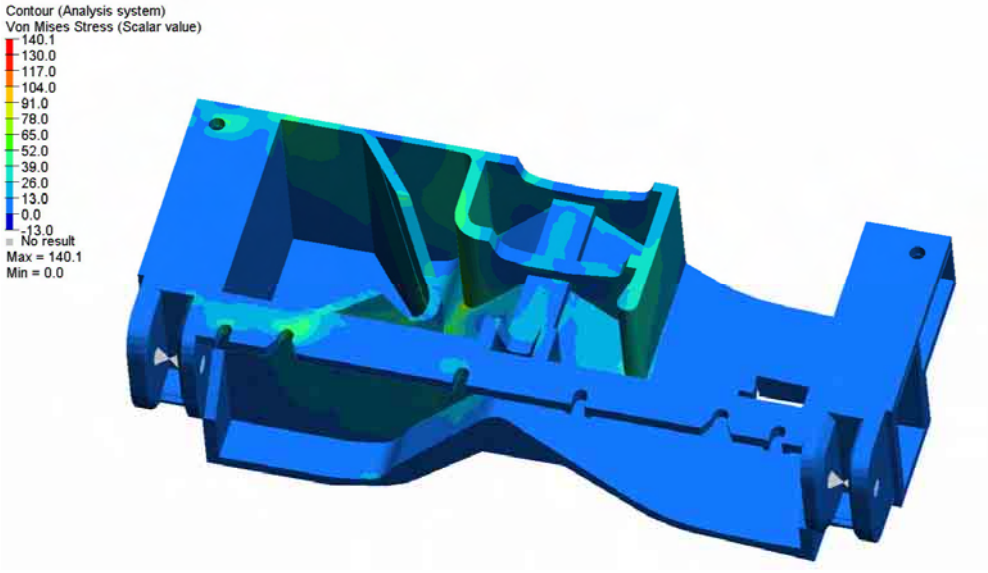

Fig 11.7 Von Mises Sress analysis of optimized die

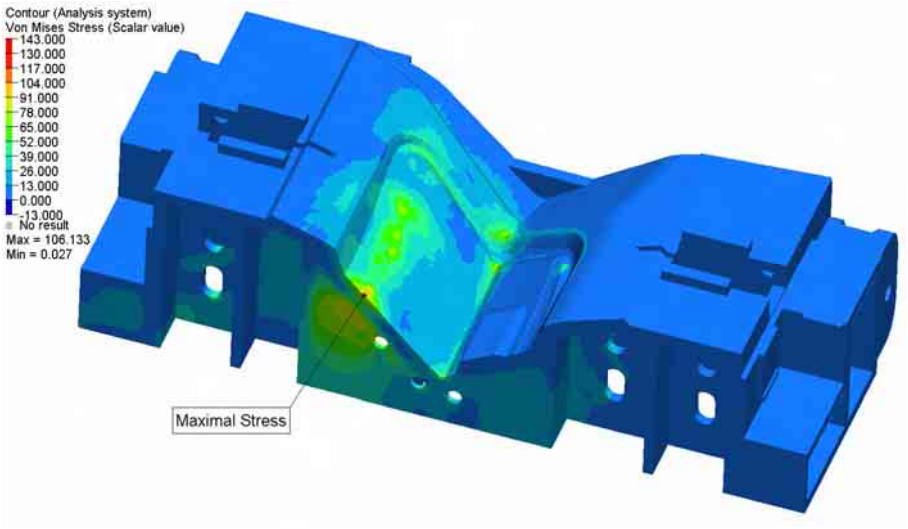

Fig 11.8 Von Mises Stress analysis of the Volvo die

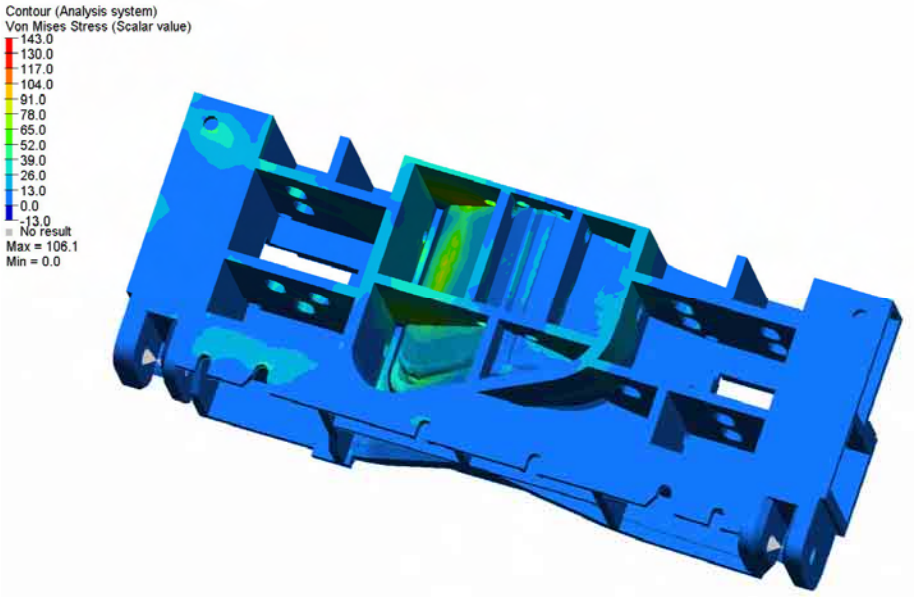

Fig 11.9 Von Mises Stress analysis of the Volvo die

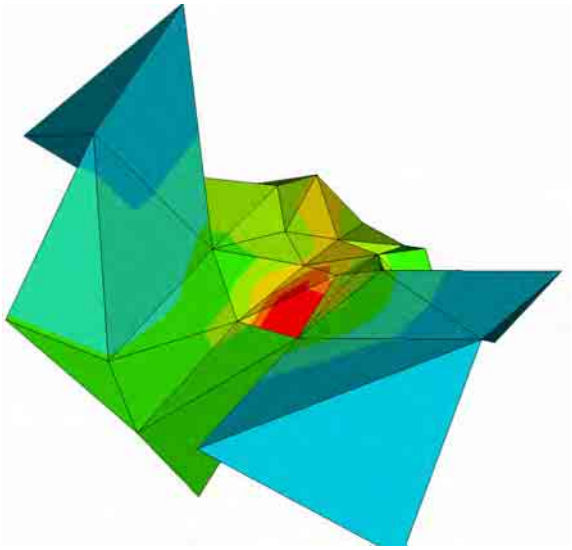

Fig. 11.10 Element exposed to maximal stresses

Chapter 12

Morphing and Final Analysis of Optimized Die

Shape changes can easily be created on complex FE-model geometries using morphing technology. The topology of the mesh is maintained when morphing, but the location of the elements will change. This means that the elements can be dragged and translated as one like, but the number of elements and nodes in the mesh will always be the same.

Topology optimization gives only a coarse layout of the boundaries of the structure. The next step is to perform a shape and size optimization. Due to the limited time of this project only a morphing study has been performed, which is a part of a shape and size optimization. We decide on the basis of the results from the stress and displacement analysis which parts of the structure that needs to be further optimized. Areas with large displacements and high stresses, as well as areas with small displacements and low stresses are of interest for morphing, since increased stiffness and further weight reduction can be made here. Figure 12.1 states these areas, where the red ellipses marks the areas where weight reduction might be achieved, and yellow ellipses marks the areas where increased material might be needed to further improve the stiffness.

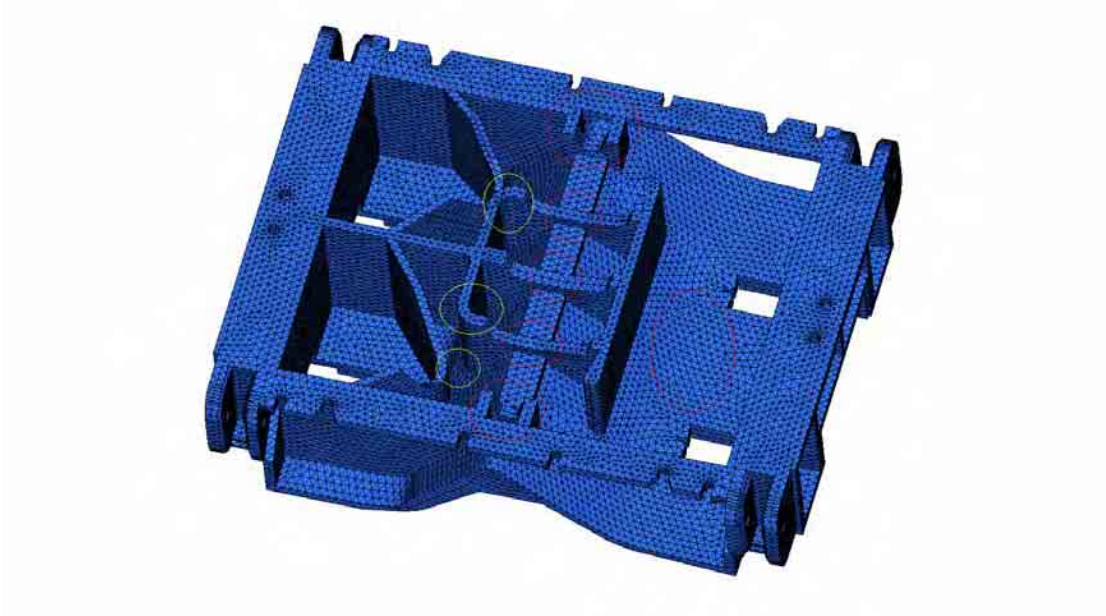

Fig. 12.1 Optimized die with morphing areas marked

We have narrowed down the width of the ribs in the spine as well as the area underneath the red ellipse to the right. We have also extruded the area with maximal displacements and enlarged the radians of the rib in the yellow marked area. Figure 12.2 shows all changes made by morphing.

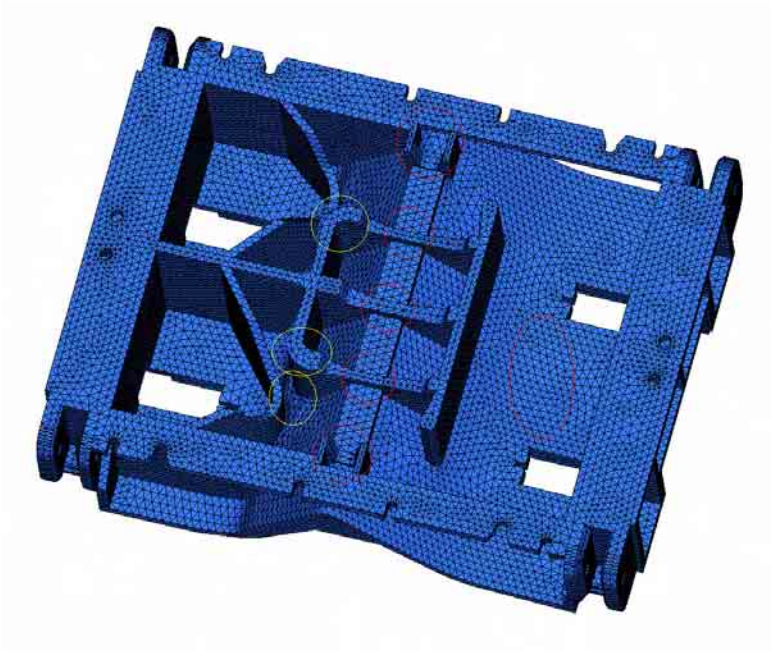

Fig 12.2 Optimized die where morphing has been performed

Yet another analysis is set up, and the maximal displacement and von Mises stresses on the morphed die are obtained. These results can be seen in figure 12.3 till 12.6.

Table 12.1 shows the numerical results in the original, optimized and morphed die. The weight of the morphed die is still 19% lighter than the original and the maximal displacement is 33% less the amount of the original. These results show that the morphing study made a great impact of the maximal displacements.

	Volvo Original Die	Topology Optimized Die	Difference	Morph Improved Die	Difference
Maximal displacement (mm)	0.322	0.275	-15%	0.215	-33%
Maximal Von Mises Stress (MPa)	106.1	140.3	+32%	140.3	32%
Weight (kg)	9605	7826	-19%	7812	-19%

Table 12.1 Comparison between original, optimized and morphed die

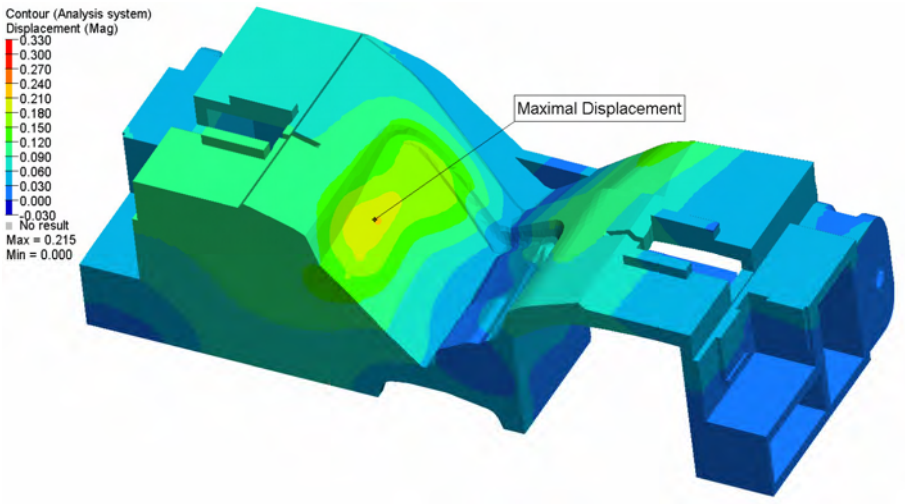

Fig 12.3 Displacement analysis of morphed die

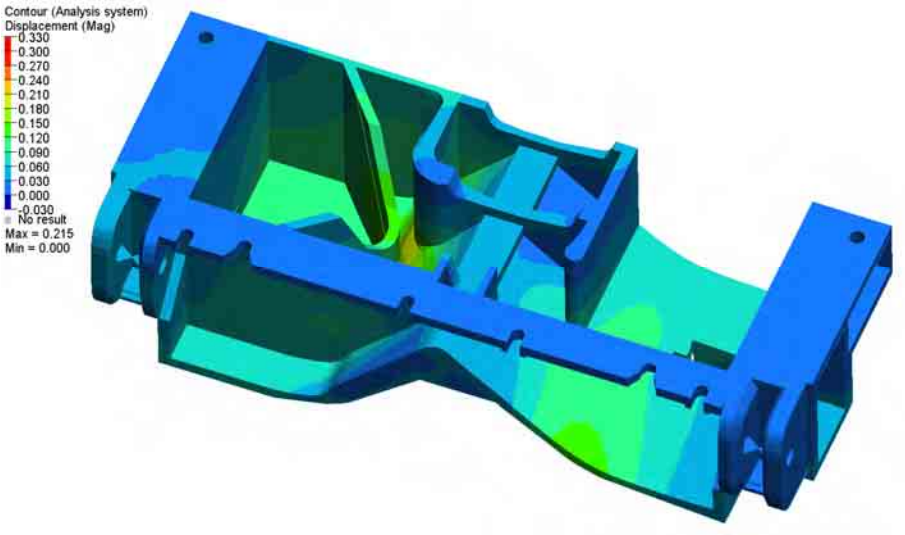

Fig 12.4 Displacement analysis of morphed die

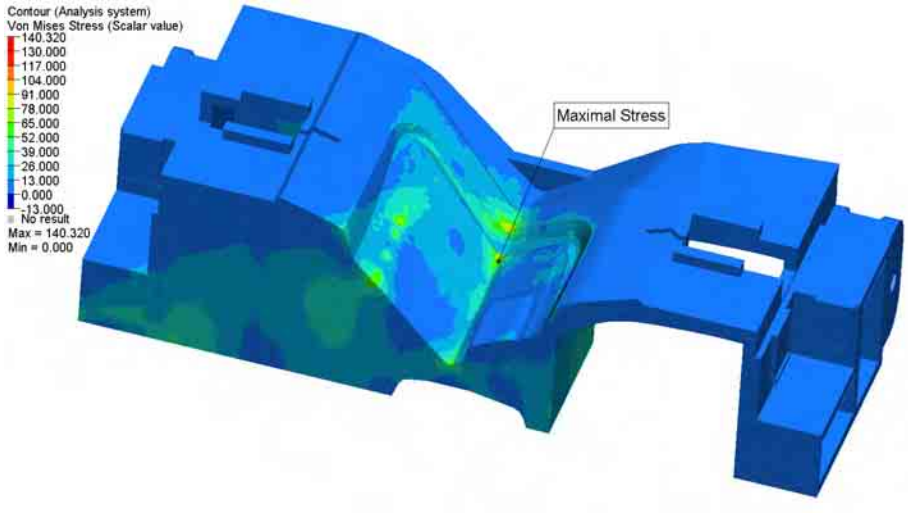

Fig 12.5 Stress analysis of morphed die

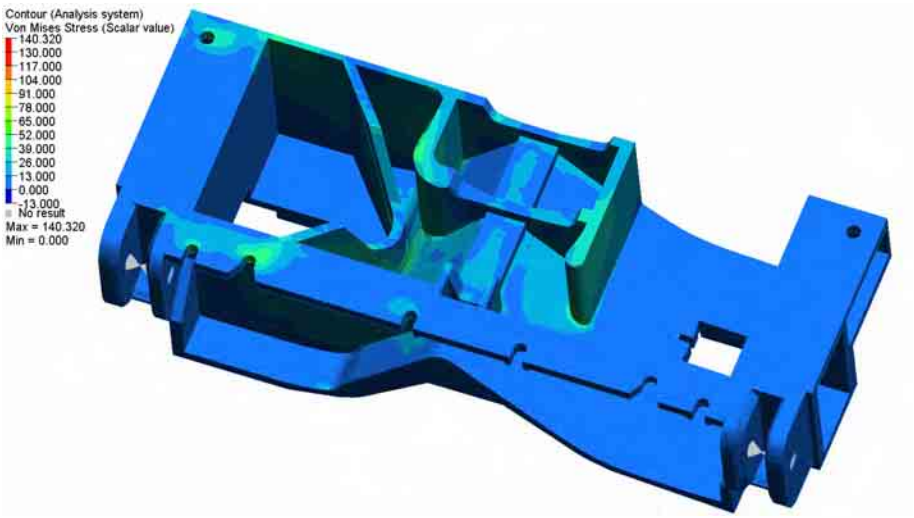

Fig 12.6 Stress analysis of morphed die

12.1 Gravity Analysis of Final Design

The topology optimized and morphed die is the final design presented in this project. A requirement VCBC has expressed is that the new design should be able to carry its own weight in one lifting lug. This is for repairing and cleaning of the tool. Therefore, analysis of the final die, when exposed to this load case, has been performed. The set up of this problem is a simple constraint in the lifting lug, which locks the tool from moving in all degrees of freedom. Gravity acts on the die in the direction from the lifting lug through the centre of gravity. Figure 12.7 and 12.8 shows the problem set up and the result of the analysis. As the result shows, the maximal von Mises stresses

occur in the hole of the lifting lug and has a magnitude of 89MPa. Since this value is beneath the yield stress of the material this is considered as reasonable.

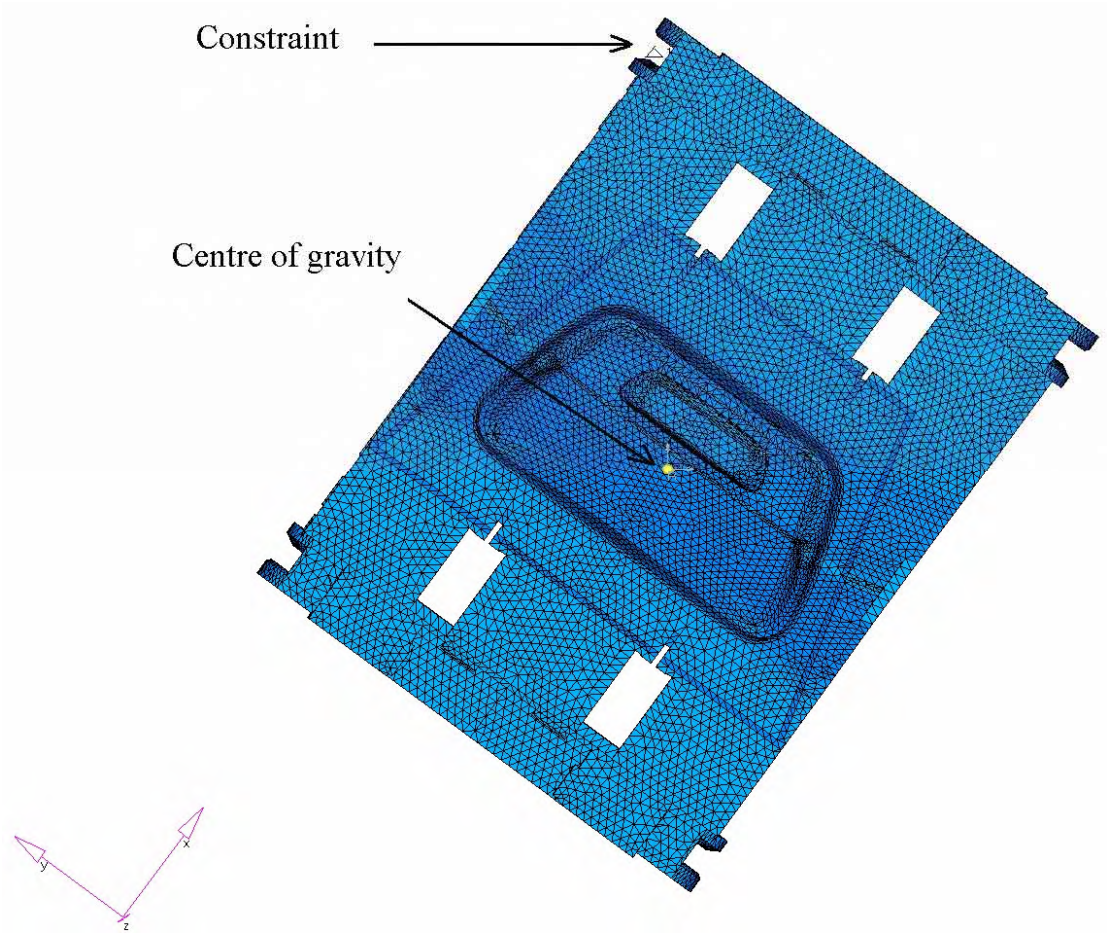

Fig. 12.7 Problem set up for gravity analysis

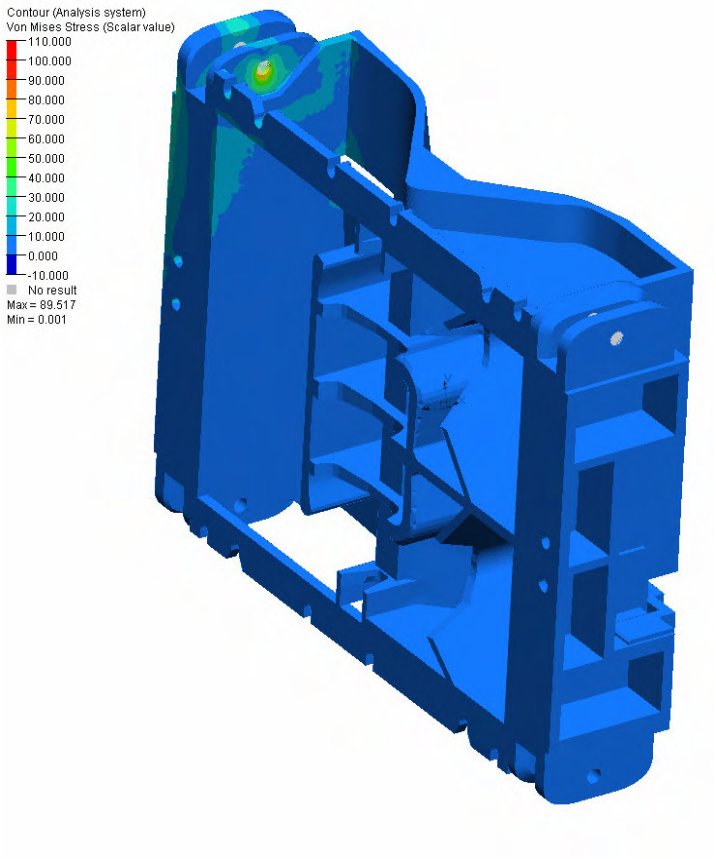

Fig. 12.8. Stress analysis of gravity case

Chapter 13

Conclusions and Discussion

This study show that a die tool of reduced weight and maximum displacement can be obtained through topology optimization, given the loads established in the forming simulation. The set up of the forming simulation proved to be more complicated and time-consuming than expected. There were some trouble retaining satisfactory result from the forming simulation, mainly due to non-optimal CAD-geometry and coarse set forming parameters in LS-Dyna. The contact pressure generated from the blankholder force needed some alteration in order to serve as a realistic approximation of the loads for the forming process.

Also, the contact pressure at the knee of the die tool is too high, caused by too great drawbead forces or too high friction force in this area, which result in rupture of the blank. Some attempts were made to reduce this effect, but in accordance with VCBC the forming simulation obtained was set to be a good enough approximation.

Great effort was made to achieve clearly marked result from the topology optimization. We elaborated with different values of the volume fraction, finding that the best results were obtained for a volume fraction of 0.15. We also found that better results were achieved when the entire die was used in the topology optimization, instead of using half of it and a symmetry plane. The symmetry plane caused a material distribution pattern that seemed to give element near this surface a higher priority.

Attempts were made to illustrate the non rigid response of the press, by placing a layer of elastic material beneath the die. However, this bed seemed to distort the defined draw direction, giving a topology optimization result that was hard to interpret.

Finally, satisfying result was obtained for a volume fraction of 0.15, when conducting a topology optimization of the whole die tool. The final structure obtained shows clearly defined ribs that were used to create a new FE-model, by first using a CAD program to redesign the tool. The new model was then meshed and the same loads that were applied in the topology optimization were yet again used to find the structural response for the newly design tool. Naturally, the same procedure was conducted with the original die and analyses were made in both cases. In comparison of the results we found that our topology optimized die had a reduced mass of 19 % and that the maximum displacement was reduced 15% compared to the original die.

From the structural analysis, it was clearly seen which areas that were most heavily loaded as well as the ones that were relatively unaffected. This information was used to do a manual size optimization by morphing the mention areas in such a fashion that improvements were made on the structural response. Without adding more mass, a further reduction of the maximal displacement was made of 33%.

To verify that the die still can be used in the same way as it is today, a complementary gravity load analysis was done. This to assure that the die still supports to be lifted in one lifting lug. The maximal stress obtained, when lifting the die in the least supported lug, was 89 MPa. Since the yield stress is 210 MPa, the morph improved die fulfils the constraints set upon it.

13.1 Future Work

An even better new design may be obtained if giving some key aspect more attention. These include:

- A limitation is that in the forming simulation the tool parts are set to be rigid, which is an approximation to facilitate the calculations. If considering the actual structural response of the die, a more accurate result may be obtained from the forming simulation.

- When considering the final topology optimized die, VCBC realised that this die might not sustain the loads on it when placed in the press. More efforts can

be made to fully describe and understand the loading cases on the die, as well as their relative relevance.

- A full shape and size optimization should be made in order to get the best result from the topology optimization. The topology optimization gives only a coarse layout of the optimal material distribution. When adding shape and size optimization to the procedure, the best attainable result should be found.

Bibliography

[1] Volvo Car Corporation Body Components, *Standard BCD 8203,004, Castings – Design instructions,* 2004

[2] *Schuler Metal Forming Handbook*, Springer-Verlag Berlin Heidelberg New York,1998

[3] N S Ottosen, M Ristinmaa. *The Mechanics of Constitutive Modelling,* volume 1. Division of Solid Mechanics, University of Lund, 1999.

[4] M Ristinmaa, N S Ottosen. *Large Strain Plasticity and Thermodynamics.* Division of Solid Mechanics, University of Lund, 2002.

[5] Bendsøe M P, Sigmund O. *Topology Optimization: Theory, Methods and Applications*. Springer-Verlag Heidelberg New York, Berlin, 2003

[6] Hallquist, J.O. *LS-Dyna Keyword User's Manual, Version 970.* Livermore Software Technoloy Corporation, 2003

[7] Maker, Bradley N., Zhu, Xinhai. *Input Parameters for Metal Forming Simulation using LS-Dyna.* Livermore Software Technoloy Corporation, 2000

[8] Kran och hisskommissionen. *Normer för Stålkonstruktioner till Kranar*, Normblad IKH 4.30.01, utgåva 3. SIS Tryckeri, Stockholm, 1981

[9] *Solid Works 2006 Online User's Guide – SP0*

Appendix A

Results of the Second Forming Simulation

Results of the second forming simulation, using different LS-Dyna input parameters, see section 7.5 for more details.

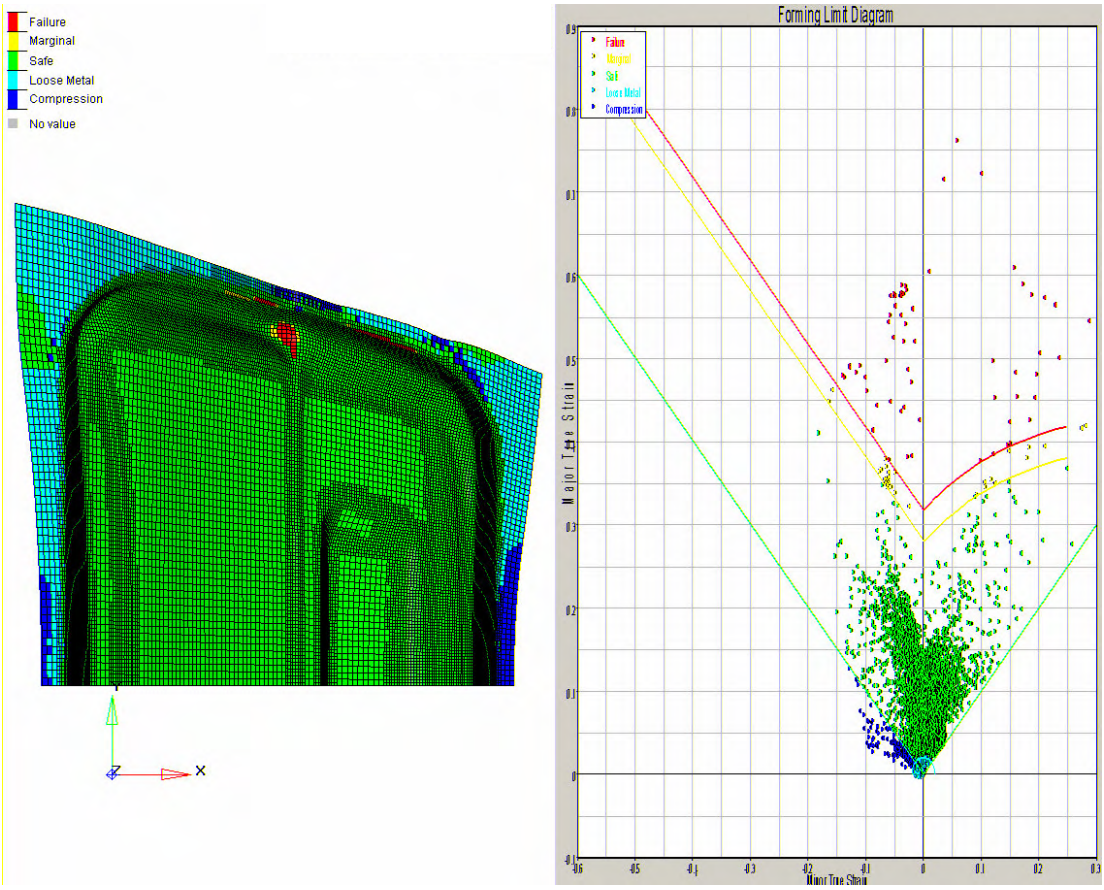

Fig A.1 FLD of the second Forming Simulation

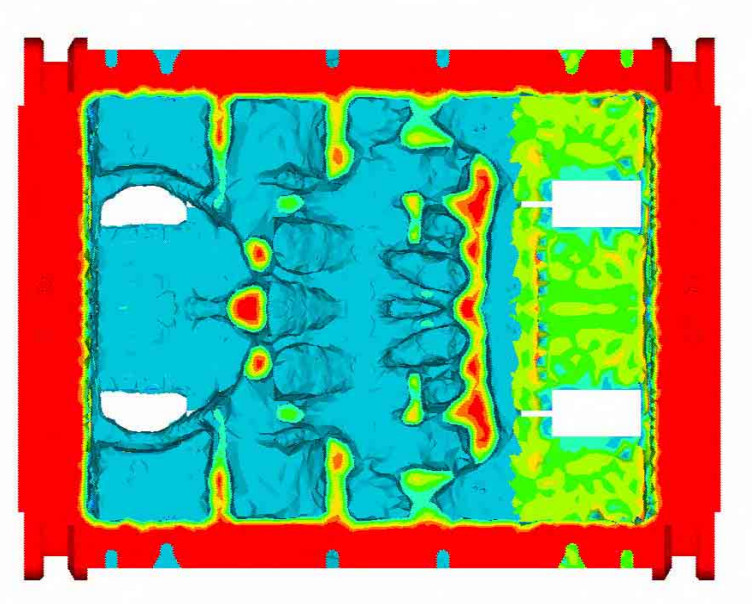

Fig A.2 Results from the topology optimization of the die with the load from the second forming simulation

Appendix B

Results of the Topology Optimizations

Results from the topology optimization of the separated loads; normal pressure, shear forces, gravity forces and the drawbead forces, see section 9.2 for more details.

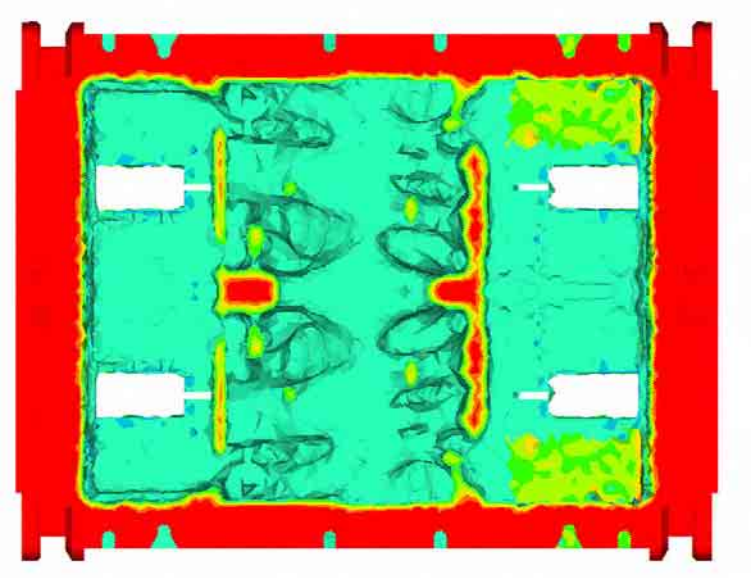

Fig B.1 Result of the topology optimization with a homogeneous normal pressure applied

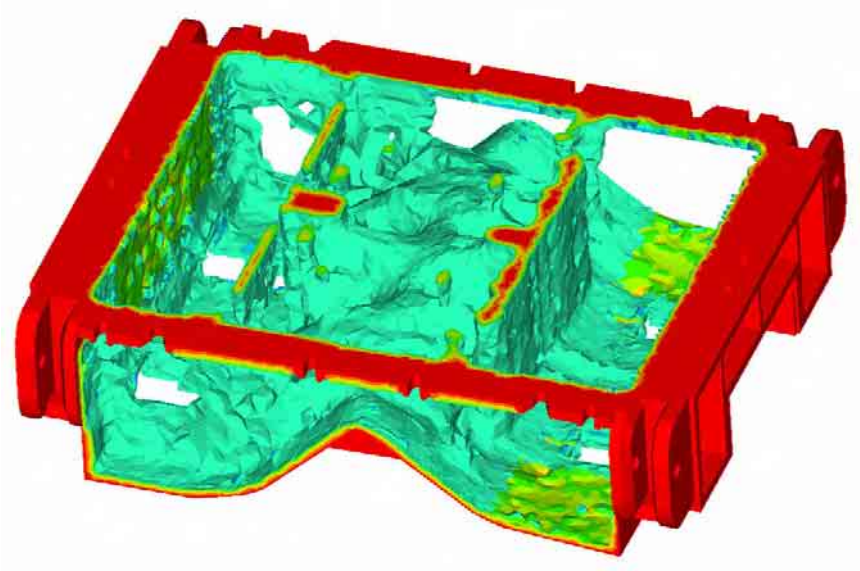

Fig B.2 Result of the topology optimization with a homogeneous normal pressure applied

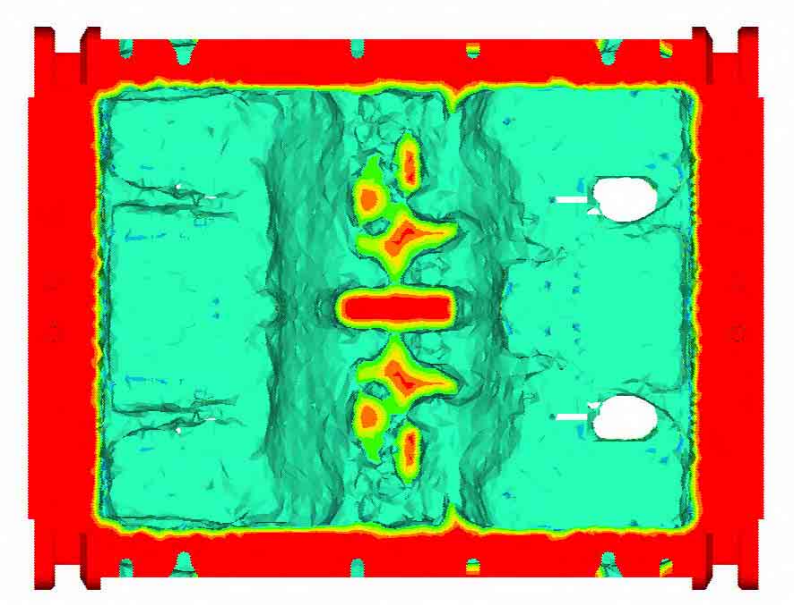

FigB.3 Result of the topology optimization with a homogeneous shear pressure applied

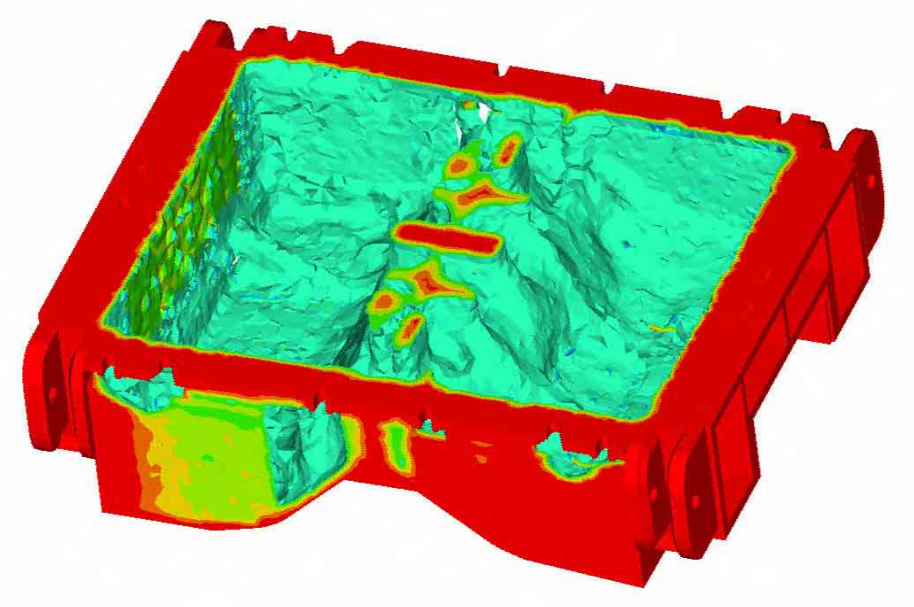

Fig B.4 Result of the topology optimization with a homogeneous shear pressure applied

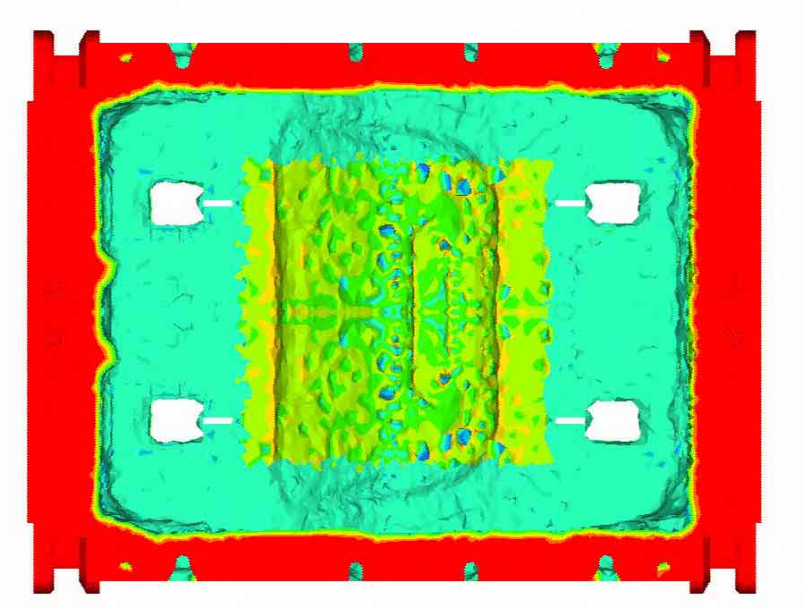

Fig B.5 Result of the topology optimization with gravity load applied

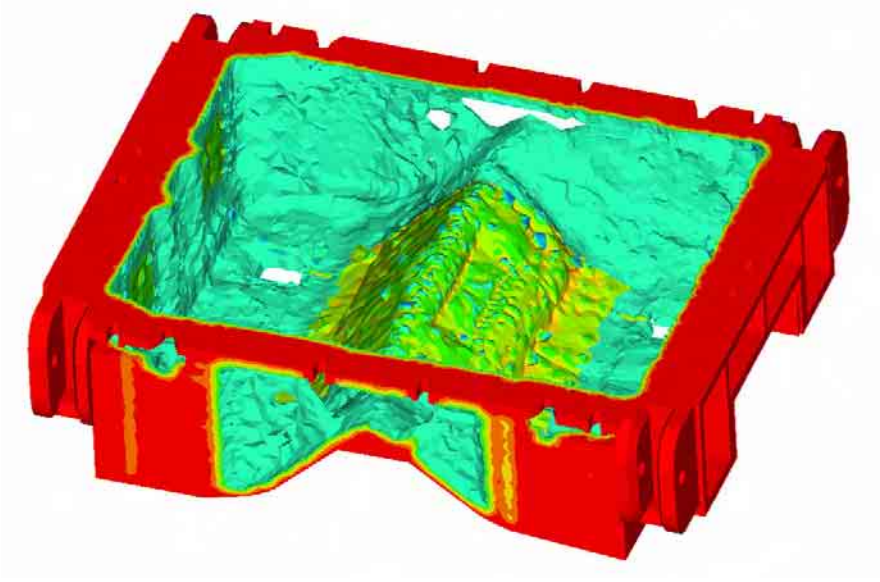

Fig B.6 Result of the topology optimization with gravity load applied

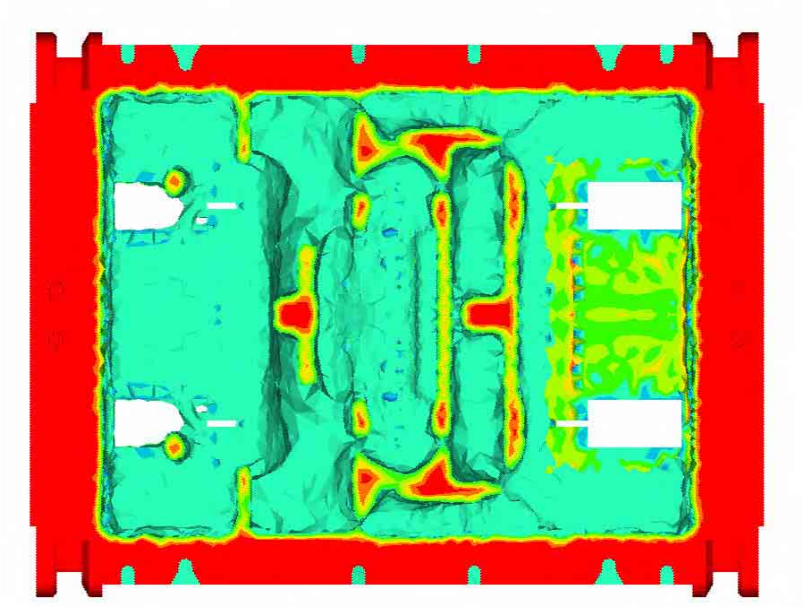

Fig B.7 Result of the topology optimization with drawbead load applied

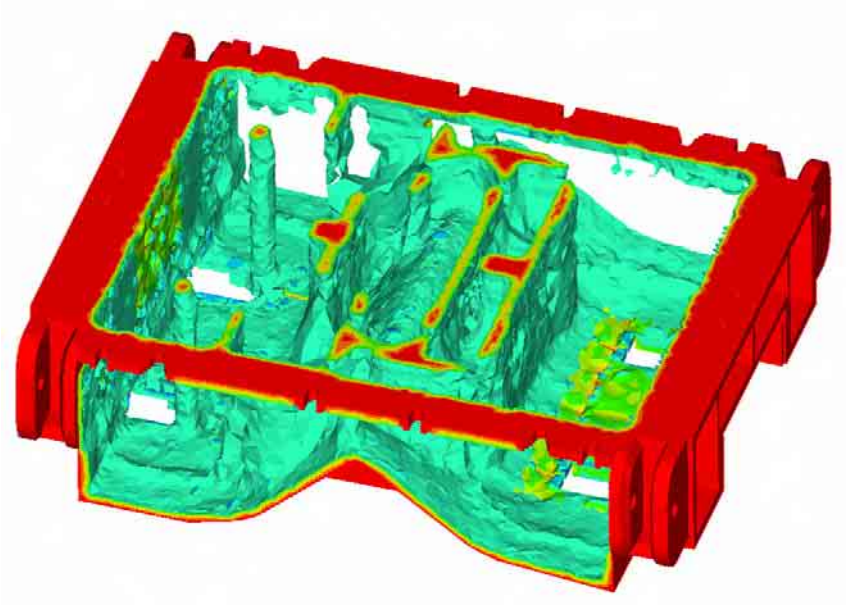

Fig B.8 Result of the topology optimization with drawbead load applied